UNIVERSITY OF
BATH

University of Bath

Alternative formats
If you require this document in an alternative format, please contact:
openaccess@bath.ac.uk

Photocatalytic foams for water treatment: A systematic review and meta-analysis

Zachary Warren, Thais Tasso Guaraldo, Alysson Stefan Martins, Jannis Wenk, Davide Mattia [*]

Department of Chemical Engineering, University of Bath, BA2 7AY, UK

ABSTRACT

Photocatalysis has proven to be highly effective for the removal of recalcitrant organic micropollutants at the lab scale. However, drawbacks such as the need for downstream removal of nanoparticle slurries and low surface areas of immobilised catalyst have, so far, hindered large-scale application. Photocatalytic foams have the potential to address these issues and advance the field towards large scale deployment. This review offers the first comprehensive overview of the state-of-the-art in this growing research field while simultaneously addressing two key issues which are slowing down further progress: The lack of classification nomenclature for foams, particularly regarding pore size and production method, and the use of kinetics as the defining feature of a photocatalyst, when alternate figures of merit, such electrical and quantum efficiencies, may be more appropriate. These were particular evident from a semi-quantitative comparison of the literature reported here, which highlighted the need for standardisation of experimental methods within the field. Finally future perspectives and best practices are discussed and recommended.

1. General overview

Photocatalysis has been extensively investigated for the degradation and mineralisation of organic micropollutants in water [1,2]. The effectiveness of photocatalysts results from a complex combination of materials properties, e.g. charge carriers' separation and the formation of oxidative species [3], and process parameters, e.g. light irradiation and mass transfer resistances [4]. Despite the promise, the industrial deployment of photocatalytic systems has been, so far, limited [5]. Nanoparticle slurries, also known as first generation photocatalysts (Fig. 1), show great photocatalytic efficiency given the high surface area in direct contact with water and irradiation [6]. However, evidence that nanoparticle release into water bodies increases the risk of exposure to humans, animals and plants [7], and that nanoparticles can leach from wastewater treatment plants [8,9], limits their use in wide spread treatment applications at larger scales due to requiring costly removal steps to prevent loss to the environment [10]. Immobilised, or second-generation, catalysts were developed to address the removal problem, but suffer from low efficiency due their lower photocatalytic active surface area [11,12]. Macroporous materials, commonly referred as foams, have been developed as an attempt to address the limitations of the previous two generations of photocatalysts [5,13].

Photocatalytic foams offer great potential in terms of efficiency, activity and, crucially, in scalability. Materials with two distinct levels of porosity, macroporous and microporous, can efficiently convert irradiated light into oxidative species to promote the degradation of micropollutants with significant advantage over flat substrates given higher surface area. The porosity, pore size and shape will also impact the transport of molecules inside the foams as the hierarchical pore structure leads to a tortuous flow [14].

While these foams have been produced in a wide range of forms and shapes, using a range of diverse approaches, they are not without drawbacks, in some instances not providing meaningful advantages over slurries and immobilised photocatalyst. Although superior photocatalytic performance is reported for foams relative to the equivalent slurries [14,15], including the removal of organic pollutants and mineralisation [16,17], most reports refer to nanoparticles grafted onto commercial foams. Despite reports of good adherence and stability of the coatings, the potential leak of nanoparticles into the environment remains an issue, limiting their practical use. The use of foams has also generated novel fundamental questions, e.g. about the different relevance of total and illuminated (or active) surface areas in microporous objects as opposed to nanoparticle slurries, or the need to revisit IUPAC nomenclature for porosity to include large porous objects [18].

Photocatalytic foams are a growing area of fundamental and applied research, and this review is the first to systematically analyse the field, not just discussing the state-of-the-art, but also attempting to provide a novel classification based on key characteristics of their structure, how foams are synthesised and their photocatalytic application and providing recommendations on how to further advance this area of research. In this review, foams are divided into three main categories according to the synthesis approach used, as summarized schematically in Fig. 2. *Supported foams* refer to nanoparticles, mostly TiO$_2$, ZnO and CuO, immobilised onto a 3D macroporous structure. *Substrate-removed foams* refer to those where the foam is used as a sacrificial template to obtain carbon-based 3D structures. *Substrate-free foams* refer to those produced via direct foaming of particle suspensions with subsequent calcination or sintering.

2. Methods to produce inorganic foams: general aspects

The synthesis of a solid inorganic foam was first reported in 1965 [19]. Since then, macroporous inorganic foams of controlled porosity have been produced using a wide range of methods, such as replica, sacrificial template, or direct foaming (Fig. 3) with average pore sizes ranging from 1 to 1000 μm [20]. The first report on the use of foams for photocatalytic applications dates to 2004 [21].

The replica technique is based on the impregnation of a suspension or precursor solution onto a cellular structure to produce a macroporous material presenting the same morphology as the original porous structure [20]. In contrast to the replica technique, the sacrificial template method involves the preparation of a biphasic composite composed of a homogeneously dispersed sacrificial phase in a continuous phase of precursors or particles which forms a negative porous microstructure after template removal [22]. The direct foaming technique is based on the incorporation of air into a suspension or liquid phase with subsequent set and drying to maintain the air bubbles within the structure. The material is usually sintered to improve strength of the final porous material [23]. Porosity and pore size are determined by the template and sintering conditions in the replica and sacrificial template methods. The porous object is the negative replica of the original sacrificial template while the replica techniques produces a positive porous structure [20]. The replica method and direct foaming either with surfactants or particles forms objects with higher average porosity (ranging from 40 % to 95 %), while the sacrificial template method results in objects with a lower average porosity with reported porosities over a much wider range (2–90 %) [20]. The overall porosity is relative to the amount of gas

incorporated into the suspension while the stability of the liquid template before setting determines the pore size [20]. Other methods to fabricate inorganic foams such as liquid templating [24–26], cast moulding and freeze drying [15], microfluidic [24] and 3D printing [27] were also reported either in combination or alone. With understanding and control of the synthesis of foams, particularly replica/template structure, volume and rate of gas incorporation and surfactant concentration [28], properties as porosity, pore size morphology and distribution can be fine-tuned [24,26].

Commercial foam supports can be divided into four main groups as metallic (such as Ni, Cu and stainless steel), metal oxide (such as Al$_2$O$_3$), semiconductor (such as SiC) [29–33] and polymeric (such as polyurethane-PU) [34,35]. Metallic and polymeric foam supports were used as sacrificial templates to produce carbon-based foams mainly composed of graphene [36] and reduced graphene oxide [37]. A few reports include other supports such as glass [38] and porcelain clay foams [39]. Immobilisation of nanoparticles onto foam supports has been the most common strategy to produce photocatalytic foams. Typical immobilisation techniques include dip coating [3,40] and impregnation [41,42].

3. Key definitions

As often happens in a rapidly developing field, the existing literature uses a very wide range of different, often contradicting, language to describe how foams have been produced, what a foam is and how they perform as photocatalyst. This hinders comparison of results and, ultimately, further progress in the area. This review provides the first attempt to provide a comprehensive framework to define, characterise and assess the performance of photocatalytic foams.

3.1. Definition of foams and porosity

Within the literature, a wide variety of material structures have been referred to as "foams", from natural sponge-type structures to highly porous powder samples [43,44]. For this review, to discuss different types of foams and to systematise the available literature, a foam is defined as *"a macroscopic object that is highly porous, with porosity in excess of 80 %, and free standing"*. This excludes powders and molecular frameworks. Therefore, the authors further suggest classifying foams into three distinct categories according to their macroscopic structure (Fig. 4).
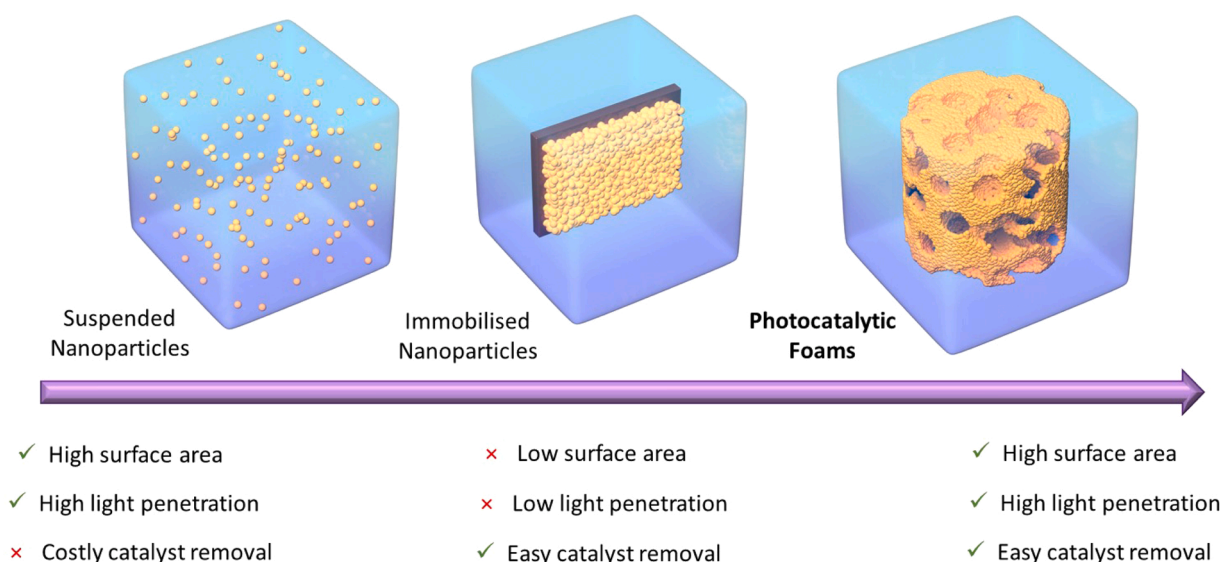

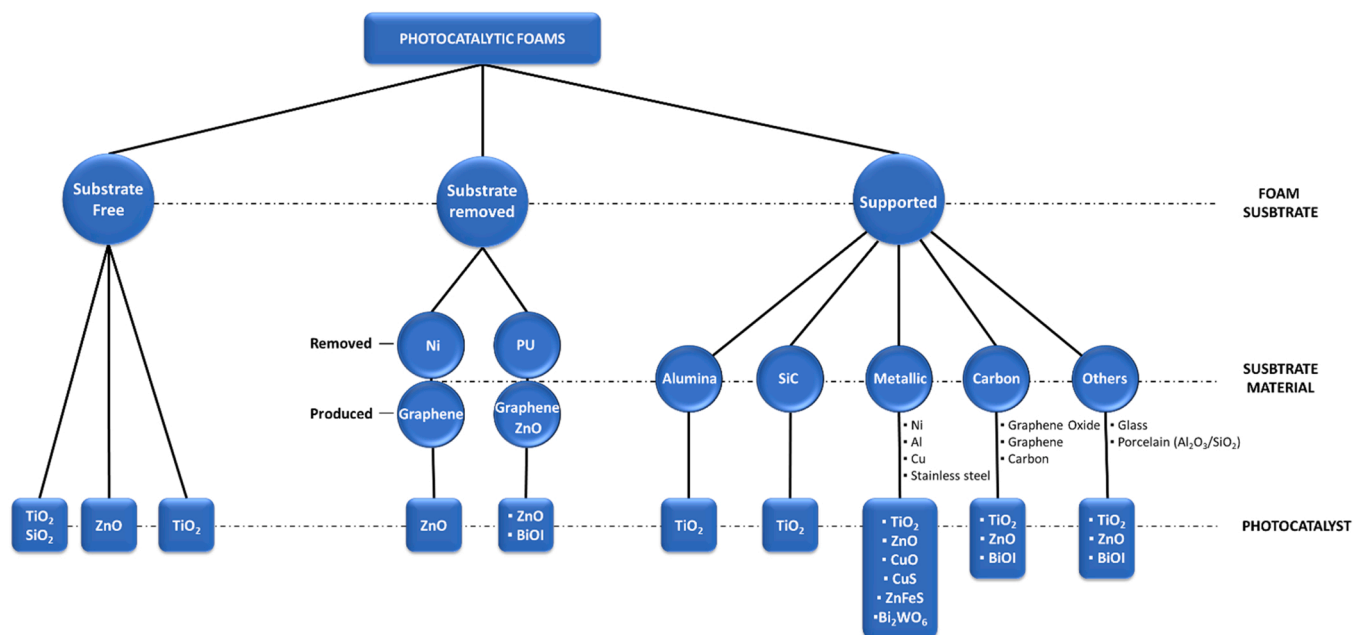**Fig. 1.** First, second and third generations of photocatalysts.

Fig. 2. Structure of photocatalytic foams for water/wastewater treatment.
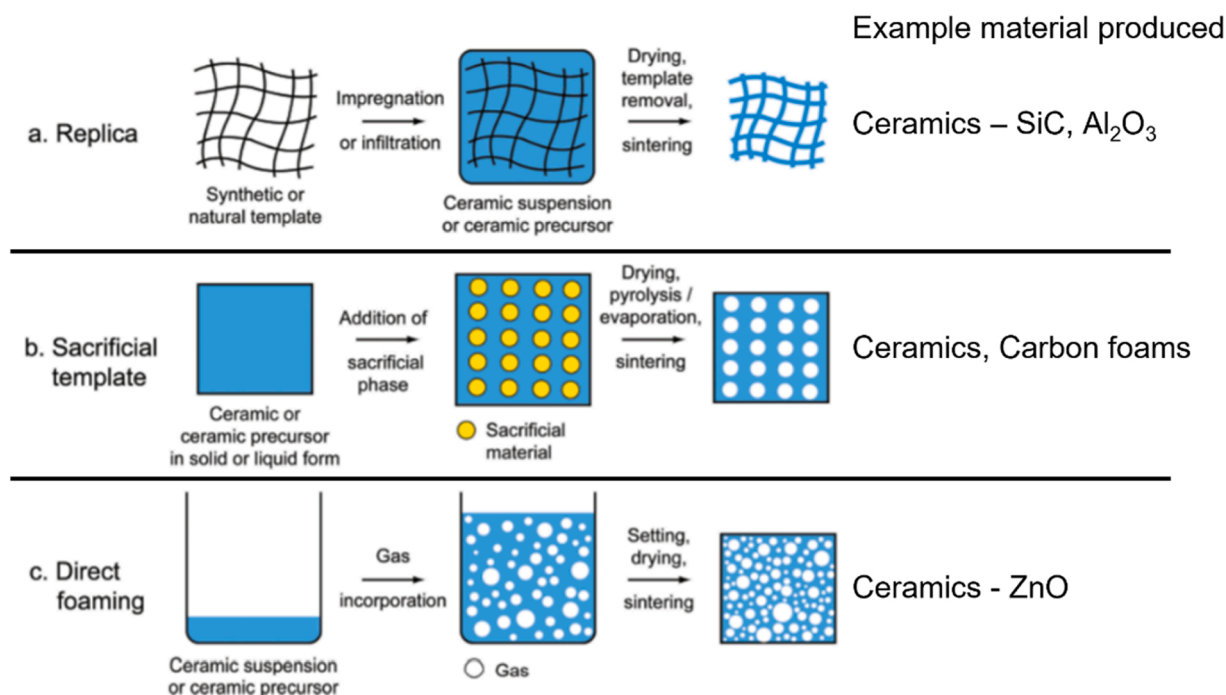

Fig. 3. Possible processing routes for macroporous foams (a) replica, (b) sacrificial template and (c) direct foaming
Adapted from Ref. [20].

(A) Foam substrates – systems where the porous structure is both extrinsic to the photocatalyst, and present in the system. These include reticulated foams of ceramic or metal materials, to which catalyst is added, leading to supported catalyst on the foam material. These systems benefit from the mechanical stability of the support material. However, a key drawback of these systems is the presence of adhered particulate at the support surface. The weak particle-support interaction may lead to catalyst leaching, impacting both the activity of the system and posing potential toxicological and environmental concerns due to catalyst loss, requiring downstream removal to prevent this.

(B) Foams formed via substrate removal – Systems where the porous structure is extrinsic to the photocatalytic material, but the support providing the structure is not present in the system. These include photocatalyst foams formed via a templating methodology onto a polymer foam, which is then pyrolised to leave only a porous inorganic photocatalyst, or systems grown on a metallic foam which is then etched. These systems often make use of graphene, graphene oxide or reduced graphene oxide and benefit
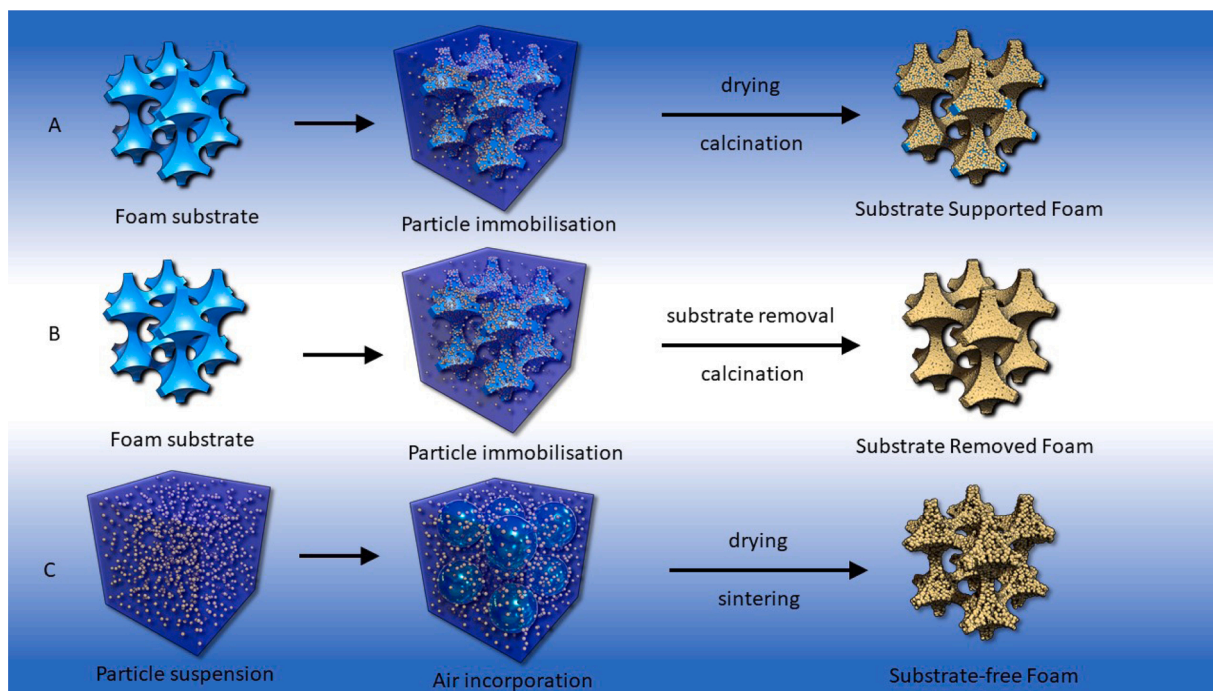
Fig. 4. Schematic representation of photocatalytic foams: (a) foams with substrates produced via catalyst immobilisation (b) foams formed via substrate removal and (c) substrate-free foams formed via direct foaming.

from the high electron mobility provided by these materials. Similar to substrate-supported foam catalysts, the presence of particles at the foam surface gives rise to the potential for leaching.

(C) Substrate-free foams – systems with porosity intrinsic to the photocatalyst, with no support present at any point in the system. These include foams produced via liquid templating or sol gel reactions. A key benefit of these systems is the lack of particle-support interactions, lowering the risk of photocatalyst loss and the need for downstream removal to prevent this. The drawback of these systems is that, as the complete structure is made of the photocatalyst materials and therefore these foams may lack the relative mechanical stability that is present when using a substrate foam as a support for photocatalyst, specifically for the mechanical stability. Furthermore, particularly in the case of ZnO foams, these systems are vulnerable to photocorrosion and methods of mitigation need to be considered in the design of reactors incorporating these foams [45].

3.2. Classification of pore size for foams – expanding upon IUPAC

Historically, the classification of pore size and pore size distribution has followed definitions set out by the International Union of Pure and Applied Chemistry (IUPAC) [18]: Micropore – to describe a pore width below 2 nm, mesopore - to describe pore widths of between 2 and 50 nm, and macropore - to describe pores with a width greater than 50 nm.

However, this system is not without faults, especially when applied to materials at the macroscale, including ceramic foams. Firstly, the IUPAC classification is based on the process of physisorption, which is affected by a wide range of factors including: pore shape, properties of the adsorptive and interactions between the adsorbate – adsorbent [46]. As a result, a distinction needs to be drawn between the porosity of the catalyst material and that of the substrate, particularly when applied to foams for photocatalysis. Both porosity of the catalyst and the substrate have different effects, and can impact catalytic activity differently, with the latter being of greater importance. Porosity leads to a higher surface area, when compared with an equivalent sized smooth surface [47]. In photocatalysis this results in a larger irradiated surface area, allowing for larger numbers of photons to be absorbed by the catalyst [48] and leading to the formation of reactive hydroxyl radicals responsible for the degradation of organic pollutants. Furthermore, the higher surface area allows for greater adsorption of pollutant at the catalyst surface, increasing overall degradation. Both aspects are well reported for both slurry and immobilised systems [49,50].

Conversely, the porosity and pore size of the foam support impact the hydrodynamics of the eluent flow through the structure, including generating a pressure and inducing turbulence in the flow [51–53]. Furthermore, the pore size has a range of impacts on the photocatalytic activity of the reactor system, with no consensus yet as to which provides the greatest benefit. Larger pore sizes offer less resistance to flow of solutions and potentially allow for greater light penetration [54–56], while smaller pores provide higher surface areas for reactions to occur at, as well as reducing the diffusion times between surface and bulk pollutants leading to greater kinetics [57,58].

As such, it is proposed that this classification be expanded to include characterisation of the pore size of objects as well as the material's properties to allow for discussions around optimal pore size of foams to occur with greater ease and frequency.

Like the traditional IUPAC method, the authors propose a three-category system for the classification of foam pore size (Fig. 5).

Foams with the average macropore size of less than 100 μm fall into the category of mini-porous foams, containing the smallest pore sizes but allowing for characterisation when these structures are expanded to macroscale objects. Most foams discussed in this review fall into the next category of midi-porous foams, foams with an average macropore size of between 100 μm and 1 mm. Finally, foams with pore sizes beyond 1 mm are categorised as maxi-porous structures.

This expansion of the classification allows for greater clarity and scope of research in both porous materials and objects (Table 1).

Most of the literature on foams as photocatalysts reports either the porosity of the substrate material, here referred as the macroporous 3D structure, or the porosity of deposited photocatalytic nanoparticles, here referred as microporosity. As both levels of porosity are intrinsically
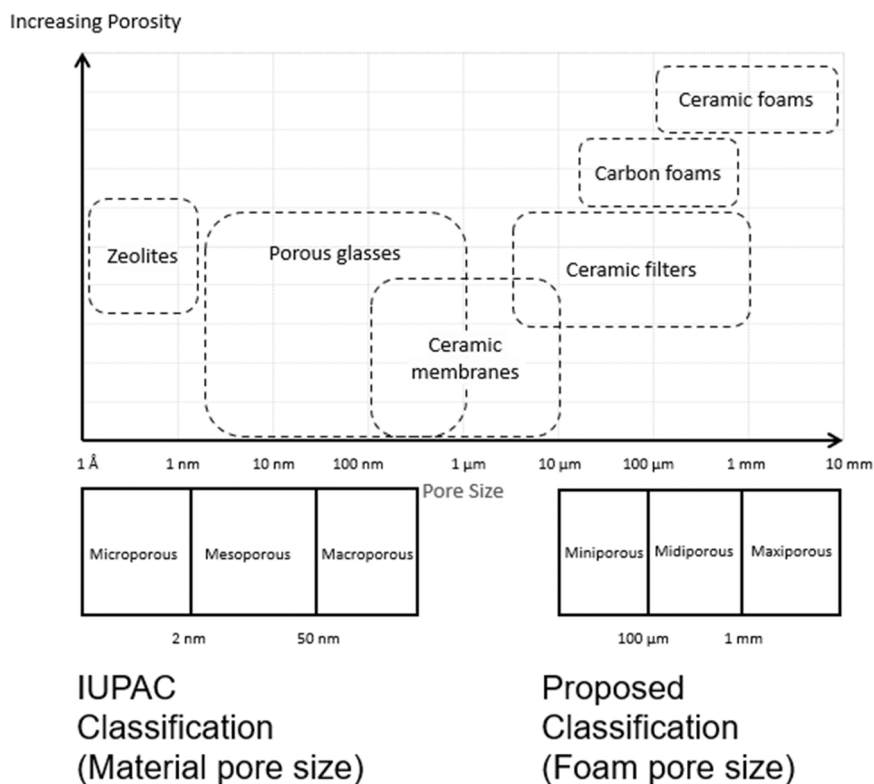
Fig. 5. Proposed pore size characterisation scheme for foams and porous ceramics. Figure adapted from Ref [59].

Table 1

Classification of foams according to the 3D macroscopic structure (foam pore size) and material microporosity (material pore size).

IUPAC Classification (Material pore size)	Expanded Classification (Foam pore size)
Microporous (≤ 2 nm)	Miniporous (≤ 100 μm)
Mesoporous (2–50 nm)	Midiporous (100 μm – 1 mm)
Macroporous (≥ 50 nm)	Maxiporous (≥ 1 mm)

correlated to the photocatalytic activity of the overall foam structure, reporting both levels allow for better understanding of properties and comparisons. Therefore, the authors propose reporting catalyst material properties, followed by support properties, for example *mesoporous TiO2 nanopowders supported on a midiporous SiC foam.*

3.3. Methodology

To facilitate a systematic review, data was collected in the following way: Concurrent data searches were performed via Scopus using search terms "foam AND water treatment AND photocataly-" and "reticulated AND water treatment AND photocataly-" to provide an initial pool of data. From this pool, entries which were duplicates, irrelevant, e.g. those using "foam" to describe a porous powder as discussed earlier, and showing no photocatalytic application or applied to gas phase photocatalysis, were removed. From this dataset, entries were assessed and those that did not report the E_{EO} or quantum yield or the parameters required to calculate them were excluded. This process was reiterated quarterly over the course of 18 months to ensure the data was up to date. After this process, out of the 81 initial entries, 32 publications were analysed with a total number of 43 data points, accounting for publications testing multiple pollutants.

Given the wide range of data, spanning orders of magnitude, logarithmic scales were applied on all figures to allow visualisation of the complete dataset. To compare and assess performances of the catalytic systems, figures are separated into quartiles, to statistically relate the performance of a particular system, within the wider dataset.

Owing to the complex nature of photocatalytic reactions, compounded by the variety of reactor set ups (e.g. batch, recirculating, continuous) and process parameters (e.g. light source, light intensity, reservoir volume, pollutant, concentration, etc.), adopting an integrated analytical framework is made difficult as each of these factors impacts the effectiveness and efficiency of the overall system.

Of particular difficulty is comparing systems using degradation kinetics alone, the most frequently used metric to assess the suitability of a photocatalyst. First, many researchers continue to use dyes for degradation studies, despite well-known limitations of this approach, such as photosensitised degradation and photochemical degradation [60], and several key articles and editorials in the literature stating that the degradation rate and kinetics of dyes systems are not truly indicative of the activity of photocatalysts [61].

This issue becomes significant, as research moves towards using more suitable target pollutants, including probe or model compounds that are more resistant toward direct photolysis, with these systems showing slower kinetics due to the absence of secondary degradations [15]. As such, a system assessed using a more photo-resistant pollutant, probe or model compound may exhibit much lower kinetics than if a dye was used, skewing the impact of research towards those that use dyes for the resulting higher kinetics, even though these may not be truly indicative of the actual performance of the system.

An approximate comparative approach is used here, using the terminology defined in the IUPAC glossary [62], allowing for a rough comparison between different systems. For different compounds used across different studies, normalised kinetics k_{ε}, wherein the kinetic rate constant min^{-1} has been normalised by the molar absorption coefficient (MAC) of the compound, M^{-1} cm^{-1} were determined. This allowed accounting for the absorption and attenuation of light, thus enabling comparison between dyes, which have high MAC values, and other pollutants which have lower values.

The authors recognise the limitations of this approach, but adopted it as the only way to provide a semi-quantitative comparison of the literature, with its wide range of pollutants, photocatalysts, reactor configuration, light sources, etc. It also further highlights the need for standardization in how experiments are conducted, and data reported, which is one of the key aims of this review.

3.4. Figures of merit in photocatalysis

In terms of the energy efficiency of the system, this review makes use of the Electrical energy per order (E_{EO}), defined as the kilowatt hours of electrical energy needed to decrease the concentration of pollutants by an order of magnitude (90 %) in one cubic metre of solution [63], and assessed using the following equations for batch and flow systems, respectively:

$$E_{EO} = \frac{P * t * 1000}{(V)(log C_0 / C_t)} \tag{1}$$

$$E_{EO} = \frac{P}{(F)(log C_0 / C_t)} \tag{2}$$

Where P is the total power output of the light source in kW, t is the irradiation time in hours, V is volume in L, F is flow rate in $m^3 \, hr^{-1}$ and C_0 and C_t are initial and final concentrations, respectively.

E_{EO} allows for an analysis of the energy consumption of a reactor system, as well as allowing for assessment of scale up potential. $1/E_{EO}$ is reported herein, for ease of understanding. The more energy efficient systems will thus have a higher $1/E_{EO}$ value.

The quantum yield allows for an assessment of the photon efficiency, assessing the number of pollutant molecules undergoing degradation relative to the number of photons reaching the catalyst surface [48]. Based on the definitions contained in the IUPAC glossary, the following equations are proposed to calculate the quantum yield of photocatalytic foams:

$$k' = (k)(C_0)(V_{Illuminated})(mol s^{-1}) \tag{3}$$

$$N_P = \frac{I_{\alpha\lambda} * S * t}{E_P} (-) \tag{4}$$

$$q_{n,p} = \left(\frac{N_P}{t}\right) \frac{1}{N_A} (mol s^{-1}) \tag{5}$$

$$\phi = \frac{k'}{q_{n,p}} (-) \tag{6}$$

where, k' is the rate of pollutant degradation (mol s^{-1}), k is the kinetic constant (s^{-1}), C_o is the initial pollutant concentration (mol L^{-1}), $V_{Illuminated}$ is the volume of pollutant irradiated.

The number of photons can be calculated using Eq. (4), where $I_{\alpha\lambda}$ is the attenuated irradiance of the light source accounting for absorbance of the medium and the pollutant molecule(s) (W m^{-2}), S is the surface of the sample onto which the light impinges (m^2) and t is the time under irradiation. $E_p = \frac{h*c}{\lambda}$ (J) is the photon energy at the wavelength emitted by the lamps, where h is Planck's constant, c is the speed of light and λ is the wavelength of light (m) from the lamps. The photon flux is the numbers of photons during irradiation of a mol of photons, where N_A is Avogadro's number (Eq. (5)). Finally, the quantum yield (ϕ) is calculated using Eq. (6).

4. Photocatalytic activity for different foam structures

The wide range of materials, supports, reactor design and testing conditions reported in the literature for photocatalytic foams makes a direct comparison between different results challenging. An extensive survey of the literature, reported in Tables 2–4 in Appendix 1, is discussed below, and based on the kinetics of the system, the electrical energy per order and quantum yields, broken down by type of foam and substrate material, highlighting the advantages and disadvantages of each system. Examples of each type of foam, along with synthetic methods, advantages, and disadvantages of each can be found in Sections 4.2 – 4.4.

4.1. Performance comparison

Fig. 6 shows a breakdown of the data compiled in this meta-analysis, highlighting the disparity between the kinetic constant of a photocatalytic system, and its suitability for large scale adoption, shown here by the inverse electrical energy per order ($1/E_{EO}$) and quantum yield. With one exception [31], photocatalytic systems that show very high kinetics (above the 75th percentile), show neither $1/E_{EO}$ nor quantum yield values above the 75th percentile. Even when considering data points above the 50th percentile, only a very small proportion of reported systems show equally high values of k_ε and either $1/E_{EO}$ or quantum yield.

Due to the initial research in the field being based on substrate supported foams, it is unsurprising that most of the data reported is based on these foams, and as such, these reports show the widest ranges, with data points falling in all four quartiles for all parameters. While these supported foams show high kinetics, when evaluating for both $1/E_{EO}$ and quantum yield, both parameters had ~50 % of the data points falling below the 50th percentile. This means, while the 3D structure of foams has been shown to be beneficial for photocatalysis due to the higher surface areas and surface area to volume ratios, this is countered by the fact that the supports are inert, i.e. non-photocatalytic, thereby limiting the effective use of the incoming light from the irradiation source, resulting in lower quantum yields [64].

Fig. 6 shows that the substrate-free foams have some of the highest values for k_ε, $1/E_{EO}$ and quantum yield. These can be attributed to multiple factors: The substrate removed foams show very high porosities (>90 %), and particularly open porosity, resulting in high surface areas that can be reached by both pollutant and photons, providing area for degradation reactions to occur at. This allows for greater utilisation of light, increased electrical efficiency and thus better performance.

Discussion on the impact of substrate removed foams is partially hindered by the low number of data points. Note, that the data available comes from systems involving reduced graphene oxide (rGO) within the foam. rGO is not inherently photocatalytic, but finds use within photocatalytic systems due to its excellent charge transfer properties resulting in longer electron/hole pair lifetimes [65,66]. This means that its inclusion likely leads to increased quantum yield of the system for a wide range of photocatalyst materials [67].

The impact of photocatalyst material on figures of merit is of particular interest. Considering quantum yields of the photocatalytic systems, foams with highest quantum yield are those made of ZnO or Zn based photocatalysts, with one exception. Foams made of TiO$_2$ show low quantum yields irrespective of foam type. This is because ZnO to absorbs over wider range of wavelengths compared to TiO$_2$, allowing for greater utilisation of available photons [68], as well as TiO$_2$ suffering from higher rates of electron hole recombination. [69].

While the majority of publications assess TiO$_2$ and ZnO catalysts, a few studies investigate the use of more complex photocatalysts, including copper oxide-based catalysts (CuO, Cu$_2$O), [33,70] and bismuth tungstate (Bi$_2$WO$_6$), [71] or oxoiodide (BiOI) catalyst [72]. The latter two provide photocatalytic activity in the visible light spectrum and may be therefore useful in solar-driven photocatalytic systems.

As one would expect, as more time is dedicated to research into the field, coupled with technological advances, the results published show an upward trajectory in terms of performance. This can be seen in Fig. 7a and b, where > 85 % of the data points from papers published between 2009 and 2014 show kinetics below the 50th percentile for kinetics, contrasted with 50 % from 2015 to 2019 and 33 % from those published
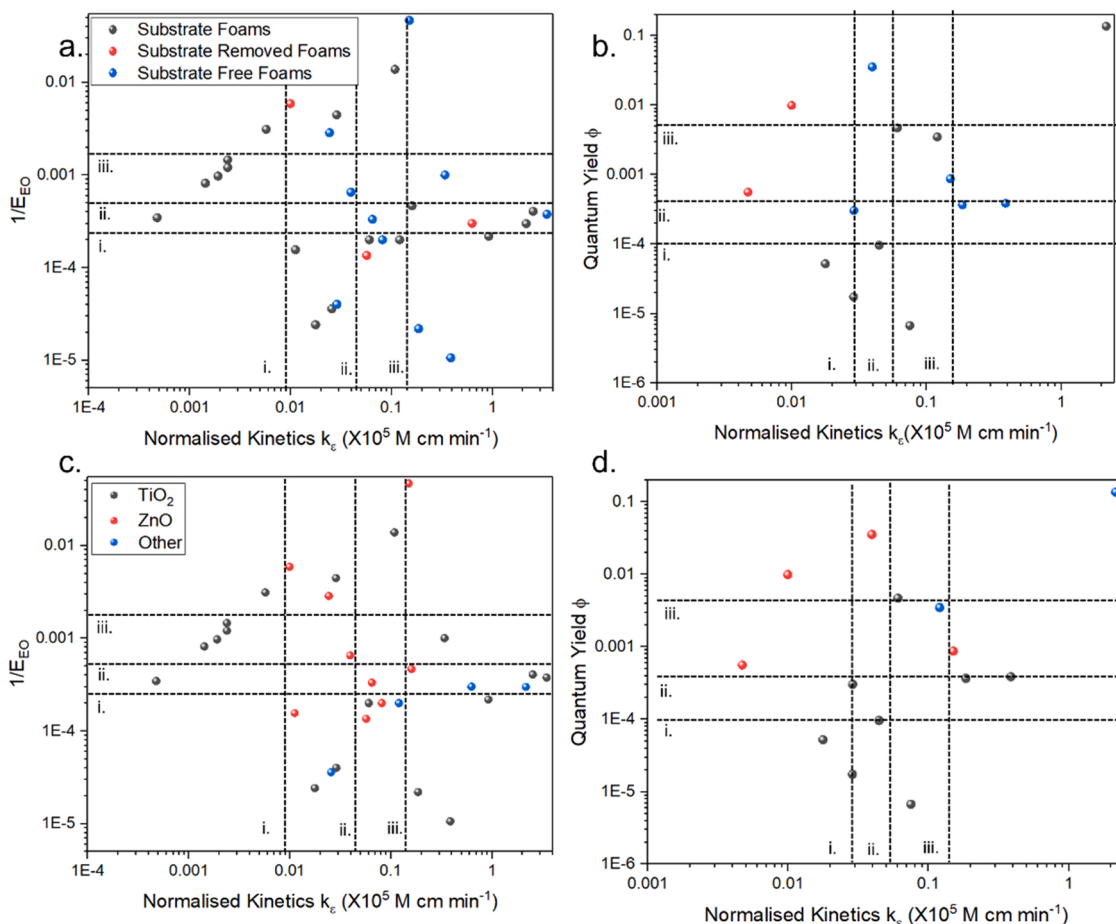
Fig. 6. Plots of left) $1/E_{EO}$ and right) Photocatalyst quantum yield, against normalised kinetics, k_ε, for foam based photocatalytic systems showing a breakdown by: (a,b type of foam and (c,d) photocatalyst material. Lines i, ii and iii represent the 25th, 50th and 75th percentile respectively. The legend in graphs a and c, also apply to graphs b and d, respectively.

since 2020, respectively.

As shown in Fig. 7c and d, the research conducted between 2009 and 2014 primarily used TiO_2 supported on foam substrates, likely due to the widespread usage of TiO_2 nanoparticles for slurry systems and the relative simplicity of production of ceramic and metallic foams [13,73, 74], as discussed previously. After 2015, publications appear to split into distinct camps: those continuing to focus on supported TiO_2 with reports of greater electrical efficiencies but with little change in quantum yields, along with higher kinetics.

This suggests main improvements were made in reactor design and photocatalysts preparation, leading to faster degradation kinetics and associated shorter times to do so, thus reducing the electrical energy per order [16]. The other camp is represented by publications focusing on Zn-based catalysts, containing ZnO and ZnFeS catalysts on substrates [42,75]. The first use of substrate-free foams as photocatalysts was reported in 2017 [15]. From here, moving into the 2020 s, the field undergoes further expansion: More research has been conducted into TiO_2 supported foams, with reporting of higher kinetics, but with limited improvements to the electrical efficiency [39,76,77]. Zn-based catalysts have also been used on substrate-removed foams, by removing the metal substrate while retaining the underlying porous structure [78]. These foams show improvements in electrical efficiency and quantum yield, compared to the earlier supported Zn-based catalysts. The higher efficiency can be attributed to improvements in reactor design, particularly regarding use of more energy efficient light sources. Substrate-free ZnO foams show higher electrical efficiencies, quantum yields and kinetics, which can be attributed to improvements from TiO_2 as discussed previously, development of reactors and the increased efficiencies that

come with a foam that is entirely photocatalytic [58,79]. A graphical depiction of this development pathway is shown below in Fig. 8.

4.2. Substrate supported foams - effect of substrate materials

For use as porous supports for photocatalysts, materials fall into three major categories: Metallic foams, alumina-based foams, and silica / silicon carbide-based foams. TiO_2 and ZnO are the most common materials grafted, coated, or deposited onto foams substrates. Other catalysts successfully coated onto foam substrates include multi-walled carbon nanotubes [78], BiOI [80], ZnFeS [42], as well as binary [71, 81,82] and ternary [33] photocatalysts. The methods for the deposition usually lead to good adhesion of the catalyst on the substrate, preserving the open porosity and, therefore, the high surface area of the foams. The main reported methods of deposition include spray coating [14], dip coating [14,29,77], and growth during hydrothermal synthesis [33,81, 83].

4.2.1. Photocatalytic activity for metallic foams

Metallic foams see widespread use across multiple areas, from aerospace engineering to biomedicine applications [84], to electrochemistry [85] to catalysis [86]. Metallic foams can be synthesised in a multitude of ways with techniques including casting within a resin mould, [87], use of a sacrificial template such as a polymer, [88] or use of a foaming agent [73].

In photocatalysis, the mechanical strength of metal foams represents their key benefit, allowing for applications in flow or recirculating systems [89]. Their high surface area also provides for high catalyst loading
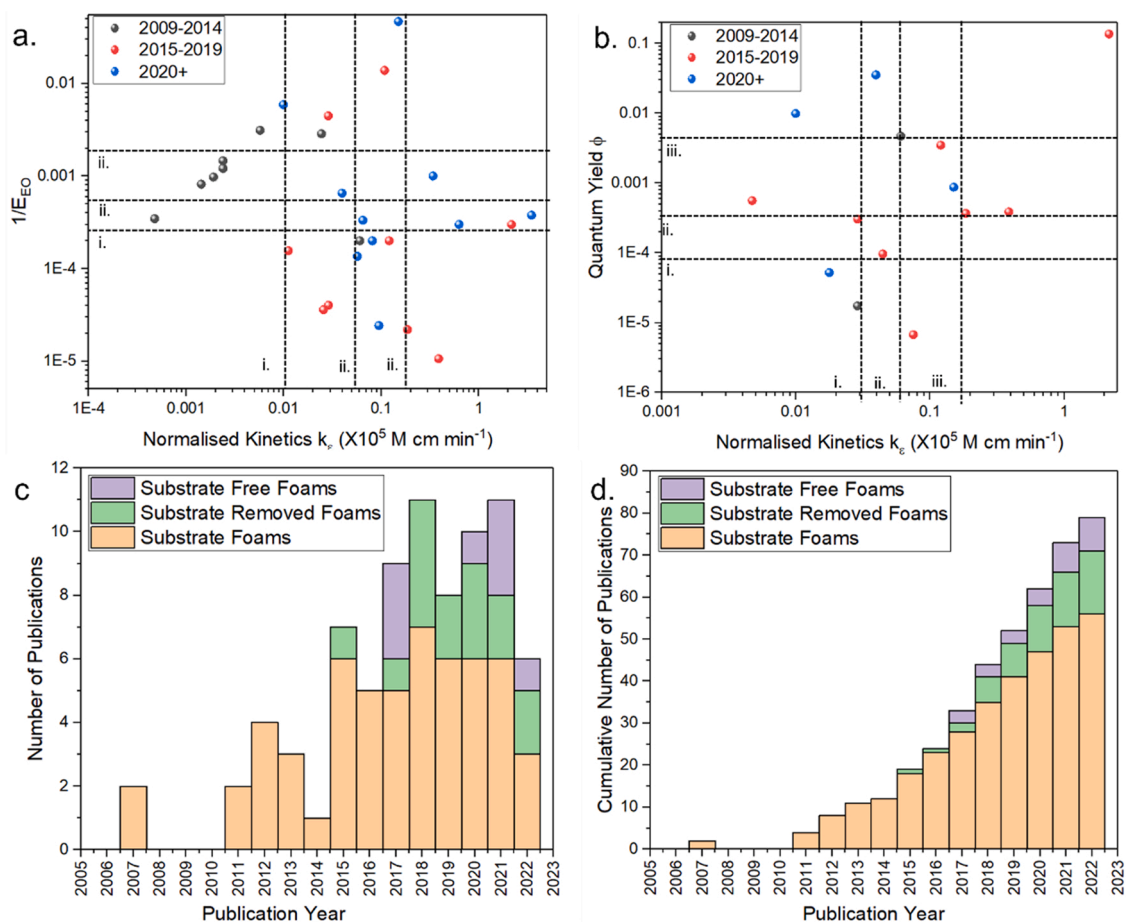
Fig. 7. Plots of a) $1/E_{EO}$ and b) Photocatalyst quantum yield, against normalised kinetics, k_{ε}, for foam based photocatalytic systems showing a breakdown by year of publication. Lines i, ii and iii represent the 25th, 50th and 75th percentile, respectively; c,d) Plots of c) annual and d) cumulative number of publications related to photocatalytic foams for water treatment broken down by type of foam used.
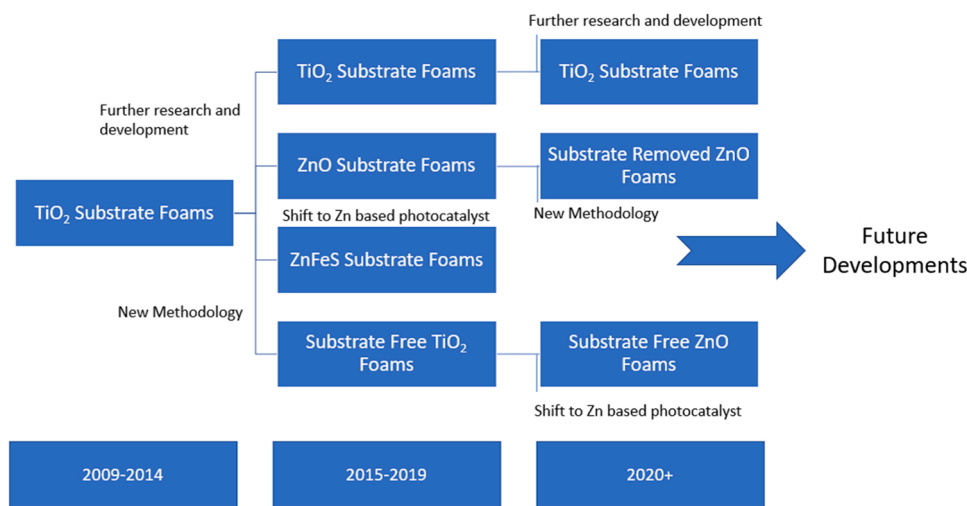

Fig. 8. Flow chart showing the development of foam based photocatalysts over time.

[73]. The conductive nature of metals has benefits when applied as supports for photocatalysts. Nickel foams have been shown to significantly increase the photocatalytic activity of supported catalyst [31]. As strong electron acceptors, the metal foams facilitate greater charge pair separation, thus increasing the lifetime of charged species at the photocatalyst surface that degrade pollutant molecules [75]. Research using

$Zn_{0.9}Fe_{0.1}S$ supported on Ni foam, showed a 6-fold increase in degradation of the fluoroquinolone antibiotic norfloxacin, when compared with an equivalence of unsupported catalyst [75] shown below in Fig. 9.

Similar findings were obtained using Fe-ZnS on Ni foams for the degradation of bisphenol A [42]. The increase in activity is attributed to the 3D structure of the foam and the high surface area that it provides,
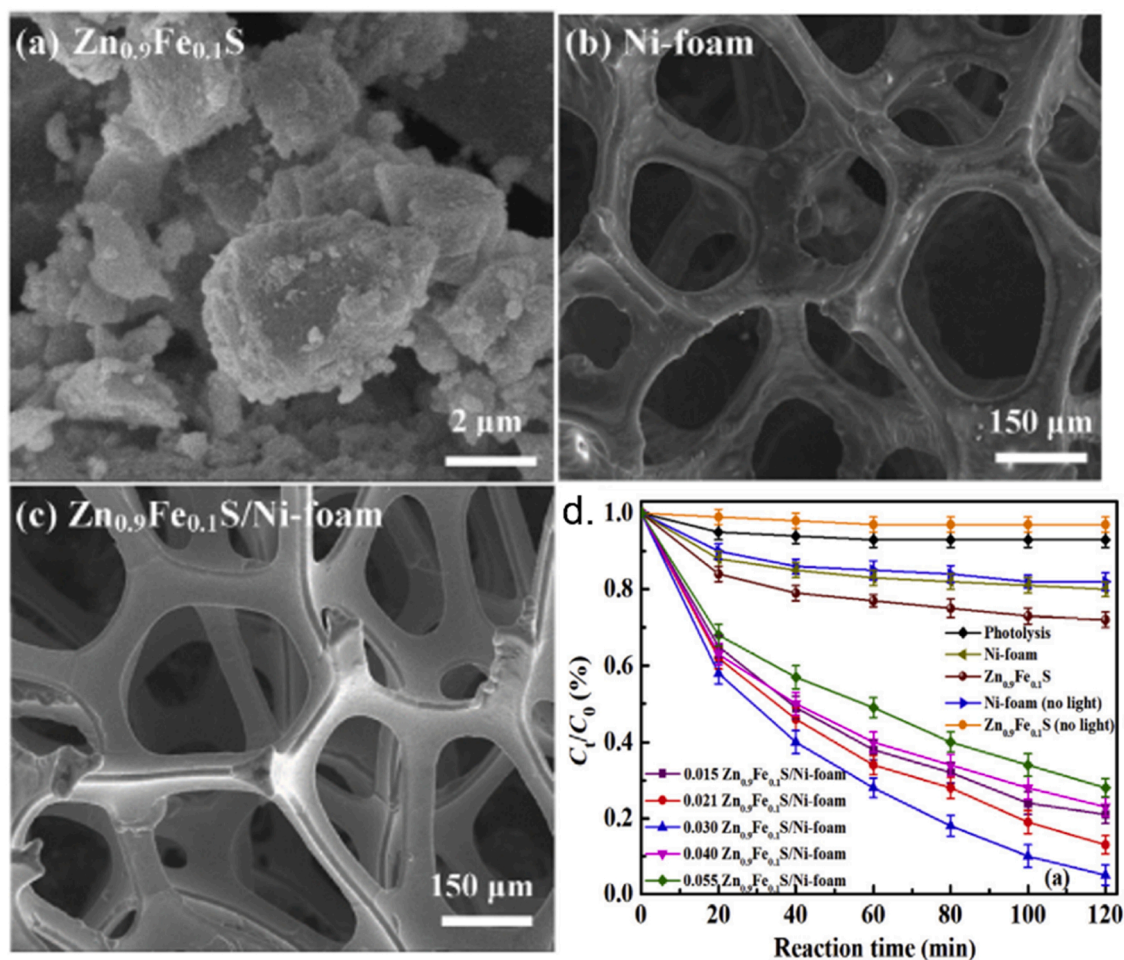
Fig. 9. SEM micrographs of a) unsupported $Zn_{0.9}Fe_{0.1}S$, b) Ni foam, c) $Zn_{0.9}Fe_{0.1}S$, supported on Ni foam. d) Removal rates of norfloxacin using $Zn_{0.9}Fe_{0.1}S$ photocatalysts.
Adapted from Ref. [75].

while also acting as an electron sink, leading to increased charge pair lifetimes. In addition, the substrate may increase the stability of the supported catalyst by reducing water-surface interaction, with both Zn^{2+} and Fe^{2+} at half the concentration leaching into solution compared with the unsupported catalyst. This, coupled with charge separation of electrons away from the catalyst surface provides a promising approach for to mitigate photo-corrosion of certain photocatalysts especially Zn-based [90].

Another beneficial effect of the use of metallic foams is the formation of interstitial oxide layers at the catalyst-substrate interface, arising as part of a heat treatment step. The metal oxide layer, particularly NiO from Ni foams, leads to the formation of a heterojunction at the surface, providing an additional route towards charge pair separation and enhanced photocatalytic activity [71,91,92].

4.2.2. Photocatalytic activity for metal oxide materials

Porous ceramic materials exhibiting high porosities currently find use in a wide range of applications including architectural infrastructure and in the biomedical sector [93], with their widescale adoption due to multiple beneficial properties including: high surface areas and permeability as well as significant mechanical, thermal and chemical stability [94]. These properties are also conducive to their use in photocatalytic flow reactors and in the decoration and coating of photocatalyst nanoparticles onto the support, as this frequently requires high temperature sintering to ensure adherence to the surface and formation of desired crystal phases of photocatalyst [95]. The synthesis of these supports

generally follows a replica-type methodology, wherein a slurry of particles is soaked into an easily pyrolised template material, e.g. PU foams, and dried prior to heat treatment to remove the template and leave the sintered ceramic support behind [13,55,96].

Alternatively, as a metal oxide, alumina aerogel foams have been produced via a sol-gel reaction using gas evolution from the decomposition of the reactants to generate porosity [97–100]. Interestingly, the surface structure of some alumina foams, particularly γ-Al_2O_3 and η-Al_2O_3, are themselves catalytic, due to the high proportion of oxygen rich groups and hydroxyl groups [101,102]. These regions provide active sites for the deposition of photocatalysts, providing strong chemical bonds and adherence to the surface of the foam [103].

With a band gap > 7 eV [104,105], Al_2O_3 is an insulating material and as such, unlike other support materials such as Ni or SiC which benefit from high electron mobility or the formation of a p-n heterojunction, its use as a support cannot provide electronic effects to promote photocatalytic degradation. Instead, alumina supports provide high surface areas for anchoring of photocatalyst nanoparticles. This gives significant performance improvement over slurries, for which it is well reported that increasing the concentration of particles in solution leads to a decrease in photocatalytic activity due to higher turbidity of the solution, negatively impacting light penetration and subsequently activation of catalyst particles [6,106,107]. For example, increasing titania nanoparticle slurry loading from 10 % to 12 % saw a decrease in kinetic constant of ∼ 48 %, whereas the same catalyst loading increase onto a reticulated Al_2O_3 led to a ∼ 450 % increase in a pilot-scale

photocatalytic oxidation reactor under UV irradiation for the degradation of tertiary amine (DBU) [14]. Similarly, complete mineralisation of phenol was achieved using TiO_2/Al_2O_3 foams with around 75 % higher photocatalytic activity than the corresponding slurry dispersion [17].

4.2.3. Photocatalytic activity for semiconductor foams

β-Silicon carbide (β-SiC) foams are highly suited towards use as foams due to their ease of synthesis, from a range of precursors, e.g. via chemical vapour deposition method (CVD) using silicon chloride and methane [108,109]. Alternatively, open cell foams of self-bonded SiC materials have been synthesised through the replica method using a polyurethane (PU) foam as template, onto which a sol containing elemental silicon and carbon black particles were deposited, followed by high temperature reaction and pyrolysis of the support [74] as shown in Fig. 10.

The high thermal stability of SiC has proved beneficial for the synthesis of composite materials, e.g. TiO_2/SiC where oxidation at high temperature has allowed tuning TiO_2 crystal structure, in particular the anatase/ rutile crystal ratio, with no change observed in the carbide support [74]. Furthermore, this stability may allow for the regeneration of deactivated catalyst, through thermal or chemical treatment, without risks of compromising the support material [94].

A particular advantage of SiC foams as supports for photocatalysis is a high density of superficial oxygenated groups, providing multiple sites for anchoring metal oxide photocatalysts to the foam [29], resulting in higher catalyst loadings than reported for other ceramic foams [14,110, 111]. A widely reported phenomena is the synergic effect between p-type β-SiC and n-type TiO_2 due to β-silicon carbides' semiconductor nature, thus allowing for coupling between the two materials to form a p-n heterojunction in the structure [112]. This results in greater charge separation, with the electrons promoted to the conduction band of the SiC moving across the heterojunction to the TiO_2 conduction band and the holes in the TiO_2 valence band moving to the valance band of the SiC [113]. This separation of charges increases the lifetime of the charged species such that the charge species have a greater chance to be involved in reduction or oxidation reaction [114]. This can clearly be seen in cases where a catalyst-free, reticulated SiC foam was shown to have low photocatalytic activity towards 4-ABS under UV irradiation with a removal of ~ 30 % after 60 h, compared with ~60 % removal using TiO_2 particles alone [110]. After immobilising an equivalent mass of TiO_2 catalyst onto the SiC foams, ~100 % removal over the same time scale was achieved [110,113]. Additionally, the photocatalytic removal of the herbicide paraquat was performed using TiO_2/SiC foams, with 90 % TOC removal achieved in a flow reactor using UV irradiation [16].

4.3. Substrate removed foams

Foams in this group are generally obtained from coating, primarily

with conductive carbon materials of a sacrificial substrate, which is subsequently removed. Commonly employed supports include metal-organic frameworks (MOFs), prepared as a template via calcination of solid architectures, obtaining clean and smooth skeleton foams, with a lightweight and interconnected highly porous structure [115]. These were subsequently coated with graphene oxide (GO) and porous ZnO nanocages, providing a superior photocatalytic activity. Similar foams were also synthesized via carbonization of starch and polyvinyl pyrrolidone (PVP). The resulting foam produced a semi-graphitized structure with high porosity where, after addition of ZnO nanorods as photocatalyst and effectively decomposed more than 98 % of rhodamine B under both visible and UV light [116].

A further example is the use of nickel-based skeletons as foam templates to generate graphene 3D structures, providing an inert and resistant substrate as shown in Fig. 11. Using commercial nickel foams consisting of a surrounded uniform close-packed macropores over the structure, a highly porous graphene foam was obtained with pores in the micrometre range and a large specific surface area [37].

The removal of the Ni scaffold from the graphene foam structure played an important role on the photocatalytic processes, with 2.5 times higher photoactivity compared to the graphene foam still incorporating the nickel substrate. This enhanced performance was attributed to the higher electron mobility of graphene and its interaction with the catalyst (ZnO). The dissolution of Ni template also increased the illumination sites on the 3D sample, improving the overall photocatalytic efficiency [117].

Furthermore, the combination of the 3D structures and the conductive properties of graphene foams can ameliorate photocatalytic processes: Reduced graphene oxide (rGO) foams grown on nickel templates showed a superior photocatalytic performance thank flat films, related to the higher surface of the structure with a more effective contact between the reaction solution and the active sites [82]. The 3D structure of GO foams allowed more target molecules to be absorbed onto the surface, reducing the light scatter by the internal pores [37]. The thickness of graphene foams can also affect the photocatalytic activity, with thicker layers of graphene compromising the mobility and electron acceptability of the foam structure, negatively affecting the photocatalytic properties of the ZnO semiconductor used as a modifier [36]. In the study, few-layers graphene was more appropriate in comparison to multi-layers, reaching a higher photocatalytic degradation of methylene blue solution under visible light illumination.

4.4. Substrate-free photocatalytic foams

A recent development in the field of photocatalytic foams is the formation of foam structures from the photocatalytic material itself, thus forming substrate-free foams. These substrate-free foams can be produced in multiple ways, including the formation of TiO_2-SiO_2 aerogels
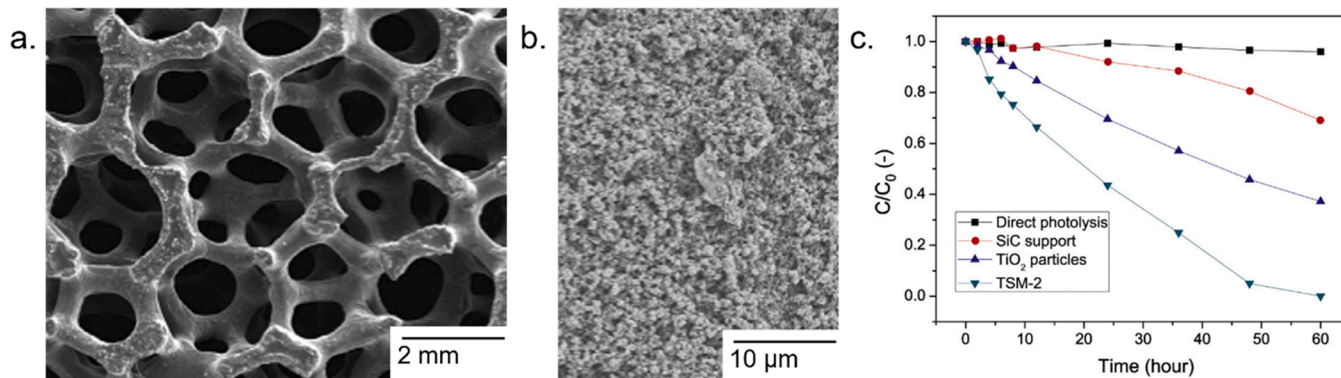

Fig. 10. SEM micrographs of a) SiC foam, b) Supported TiO_2 on foam and c) removal rates of 4-ABS using supported TiO_2 photocatalysts. Adapted from Ref. [110].
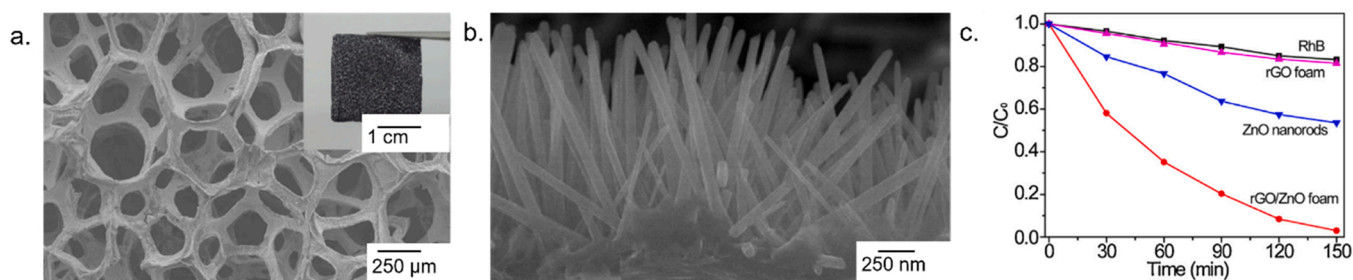
Fig. 11. SEM micrographs of a) ZnO/rGO foam (inset is the photograph of free-standing ZnO/rGO foam), b) ZnO nanorods on the ZnO/rGO foam scaffold and c) removal rates of RhB using ZnO/rGO foam.
Adapted from Ref. [37].

[118], hydrogel formation [119], freeze drying followed by template removal [15] as shown in Fig. 12, liquid templating followed by sintering of metal oxide particles [79] and direct foaming of sol-gel syntheses [58]. When compared with synthesis methods for other types of foams, which involve the use of high temperatures (e.g. for metallic foams, [73]), or the use of highly caustic reagents (e.g. for the removal of Ni foams for substrate removal, [36,82]), these synthetic methods require milder conditions and reagents for foam production.

Furthermore, the very low densities and high porosities of these foams (> 90 %) cause these foams to show buoyancy and as such are easy to replace and remove from reactors. The formation of low density, floating black-TiO_2 foams, has been reported, with the freeze drying synthesis forming a structure of both open and closed pores, with the buoyancy attributed to the latter [15]. While too many closed pores are less desirable due to the catalyst surface being inaccessible, the reported foams still showed excellent removal performance for the degradation of a range of organic pollutants including hexadecane, phenol, atrazine, rhodamine B and thiobencarb. The foams demonstrated better removal performance for all substances than the P25 TiO_2 powder reference [12]. Substrate-free ZnO foams synthesised by liquid templating and sol gel methods, applied for the photocatalytic degradation of carbamazepine show better quantum yields and energy efficiency than immobilised and slurry systems, further highlighting the benefits of the 3D foam structure [58,79].

5. Use of photocatalytic foams in reactors

The design of photocatalytic foams is intrinsically linked to the configuration of the reactors they are used in, with different designs of the latter used to make full use of the former's physical properties, particularly their 3D structure and high surface areas. Photocatalytic reactor design challenges include: (1) increasing mass transfer between the aqueous medium and the photocatalyst surface for greater kinetics; (2) maximising light efficiency and irradiation of the entire foam, due to the structural complexity of the foams, while maximising the

illuminated (or active) surface area; (3) increasing long-term stability of the photocatalyst on the substrate/template foam for use at scale, avoiding leaching and, in view of potential use, with minimal downtime caused by replacement or repair [120,121].

There is a wide range of foams photoreactors designed for water treatment, their configuration comprising continuous, batch and semi-continuous systems. The vast majority consist of simple batch systems, with the foam located in a single tank reactor with the aqueous solution being continuously stirred. However, this configuration does not take advantage of the high porosity and interconnected 3D structure of foams, which are better suited for flow reactors, where the liquid phase can permeate through the pores into the internal structure of the foam [29]. In this case, the flow can operate in a re-circulating or single pass mode with uniform mixing, with the contaminant in close contact with the foams' surface. Moreover, the flow through the tortuous structure can generate turbulence improving mixing, thereby improving the mass transfer by decreasing the external diffusion layer [14]. In a typical flow reactor, a glass tube (quartz or borosilicate) is filled with a photocatalytic foam and surrounded by UV/visible lamps, where the liquid can flow through the foams by a circulation mode using an external pump. In terms of configuration, a recirculating flow reactor is considered a versatile system for evaluation of the photocatalyst, reactor geometry, irradiation source, and fluid residence time, which can provide a simpler solution than slurry reactors [121,122]. Furthermore, it allows for the catalyst to be applied under conditions like what would be used at scale, in this case single pass flow systems [123]. Operating under recirculating conditions allows for evaluation of catalyst performance at varying flow rates and assessment of mechanical stability.

Most of the foams applied in flow systems so far have been prepared using alumina or SiC [124], which have a miniporous reticulated structure, usually at the micrometre range, and are considerably more resistant than polymer or carbon foams. The latter show lower mechanical stability and are less suitable at present for use within a flow reactor. Alumina- and SiC-based foam can be adapted to different geometries to maximise flow rate without significant increases in pressure,
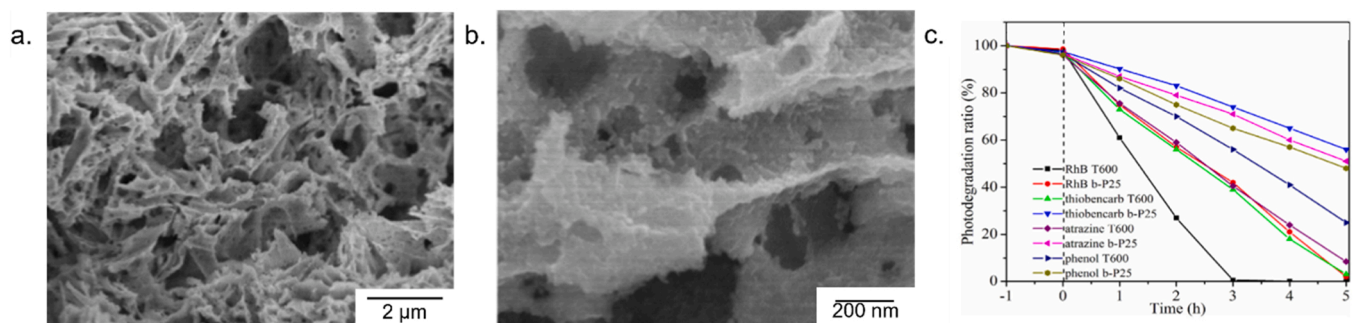

Fig. 12. a,b) SEM micrographs of TiO_2 foam and c) removal rates of multiple target pollutants using TiO_2 photocatalysts.
Adapted from Ref. [15].

which would negatively affect the energy efficiency of the reactors. Metallic foams also exhibit a highly resistant structure which make them suitable for use in flow reactor systems, but the cost to generate an open cell monolith is still considerably higher than for ceramic foams [125].

The main challenge in the design of photoreactors remains light efficiency, specifically the difficulty of providing a uniform light distribution over the whole 3D structure of the foam with sufficient light penetration to its internal core [126,127].

To overcome this challenge, different configurations have been developed, including an annular reactor, wherein the irradiation source is internal and central to the foam, positioned between the light source and the internal wall of the reactor [14]. These reactors ensure that the core of the foam is irradiated, as it is closest to the light source, but therefore, the exterior surfaces now require additional irradiation. A clever alternative has been to use a reflector, a screen made of highly reflective material such as aluminium, wrapped around the outer wall of the reactor [128], reflecting photons that passed through the foam back into the reactor and foam structure, increasing the quantum efficiency of the reactor.

An alternative strategy for the configuration of the reactor was to allocate the irradiation source through the foam, internal but not centrally. This allows for multiple irradiation sources to be included within the foam, enabling greater light coverage and higher illuminated surface areas, while providing for lamps of smaller diameters to be included, thus maximizing the illumination area and reducing the dimensions in a tubular configuration [129]. The decentralization of irradiation means that, with design and simulation, an optimal number of irradiation sources can be applied throughout the foam structure to allow for high illuminated surface areas [130].

A third strategy is to position the catalyst inside of a tubular quartz tube surrounded by the light source(s) placed externally. This methodology warrants the greatest control over irradiation, light intensity, and power usage of the reactor, through designing the reactor for light sources to be placed outside the tube at varied distance from the tube
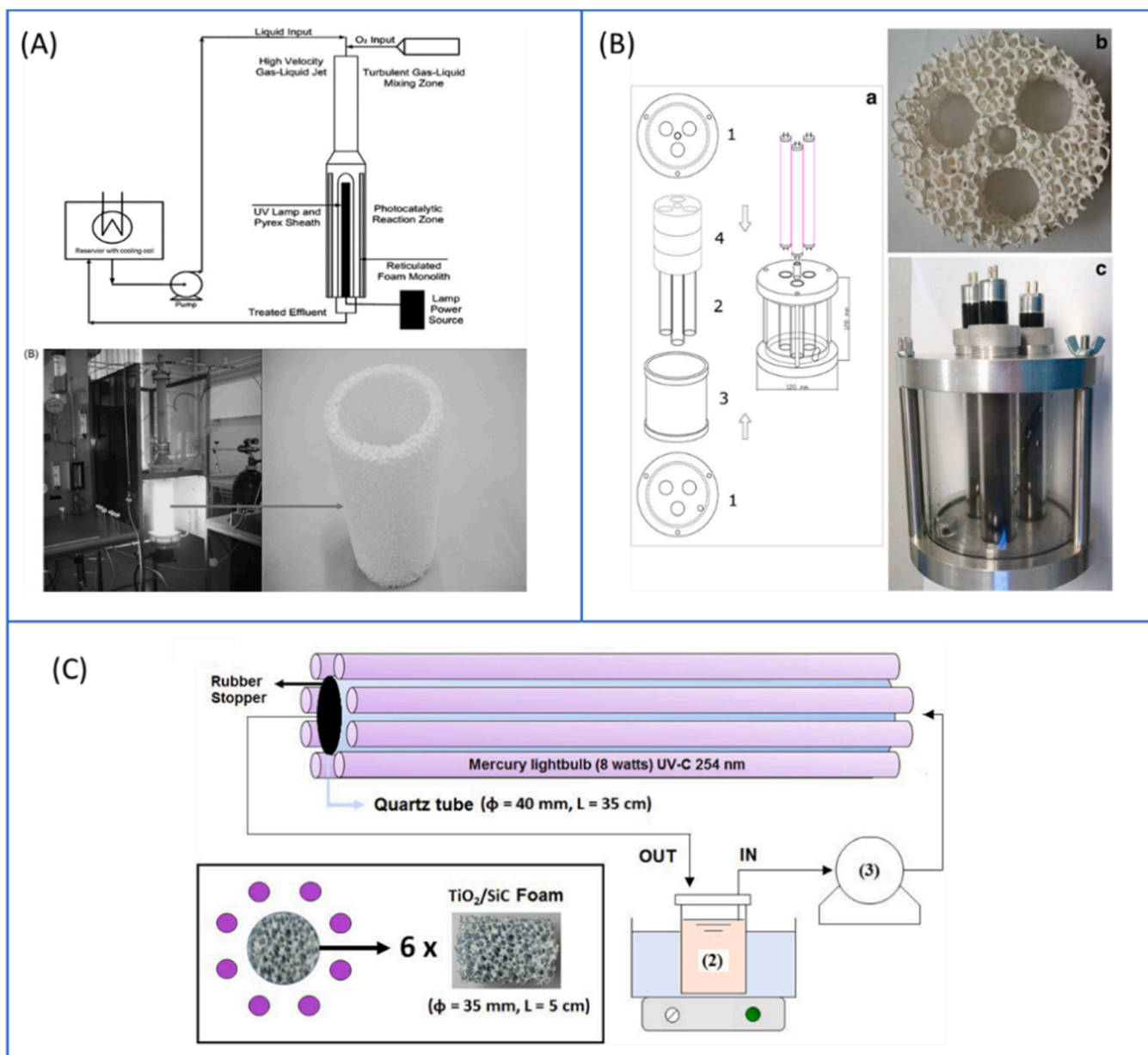

Fig. 13. Recirculating batch reactor configurations for photocatalytic foams: (A) the irradiation source is allocated internally and centrally, surrounded by a photocatalytic foam [14]; (B) designed foams allowing the presence of multiple illuminating points internally to the structure [129]; and (C) a foam centrally allocated with UV lamps externally surrounding it [111].

[111]. However, as it the only design with an external irradiation source, the use of a reflector is more complex and less effective, reducing the efficiency of the irradiation. Examples of reactor designs can be seen in Fig. 13.

The source of irradiation and how the catalyst is allocated are critical parameters that can impact the design and geometry of photocatalytic reactors for immobilized catalysts [122]. In the case of photocatalytic foams, their complex, 3D shape must also be taken into consideration as it directly affects mass and radiation transfer limitations when considering scale-up.

6. Future perspectives on development of photocatalytic foams

As shown in Fig. 8, the field of photocatalytic foams has been constantly developing, from supported TiO_2 foams to the variety of foams discussed herein, and this is likely to continue. While development thus far has focused on new methodologies for foam production, or improving the activity of photocatalysis, future developments could be expanded to include technological advancements as well.

6.1. Technological advances

Of particular interest is the application of UV-LED lamp technology that may provide significantly improved energy efficiency of photocatalysis, offer new reactor designs given the small size of LEDs compared to traditional mercury (Hg) lamps, and more sustainable lamp disposal as LEDs do not contain toxic materials as illumination source and lower energy consumption (potentially lower E_{EO}). [131,132]. While not the focus of this review, it is worth noting that these advances will bring these benefits all light driven advanced oxidation processes as well as water treatment.

6.2. Novel foam materials

Alongside the technological development, material developments will likely continue, expanding into two new fields, increasing the number of photocatalyst materials applied as foams and the use of doping materials: While most materials used currently are large band gap semiconductors, requiring UV irradiation, a common method for band gap engineering of nanoparticles is doping and has shown promise in allowing for visible light utilisation of ZnO and TiO_2 [133–135]. Non-metal dopants such as nitrogen have been shown to allow for visible light (or solar) photocatalysis of both ZnO [136] and TiO_2 [137,138], along with metal dopants such as copper [139], allowing for utilisation of photocatalysts under visible light. However, thus far these developments have been limited to modification of nanoparticle or film based photocatalysts and not been applied to foam photocatalysts in any form.

Graphitic carbon nitride (g-C_3N_4), has shown good visible light activity for degradation of pollutants [140–142], and is therefore a possible candidate for photocatalysts used for water treatment. Photocatalytic systems that utilise g-C_3N_4 thus far use it in a slurry system. Immobilisation of g-C_3N_4 onto a foam or production of a foamed variant of g-C_3N_4 would prove to be a system of interest. Furthermore, the photocatalytic activity of g-C_3N_4 systems can be tuned via doping [143].

As previously discussed, the use of substrate-free foams shows great promise for practical application and the synthetic procedures to make these foams (e.g., sol-gel, direct foaming) have potential for incorporation of dopants into the foam structure, via control of the molar % of dopant in the foam formulation.

6.3. Foam reactor development

As discussed briefly previously, the application of foam based photocatalysts in reactors requires particular care be taken with the positioning of irradiation sources as well as accounting for the 3D structure of the foam, such as pore size and illuminated surface area. As the field develops and the use of these reactors become more widespread, it is likely that these parameters will be more easily controlled leading to increased performance of the reactor, in terms of photocatalytic activity, energy efficiency and quantum yields, due to maximised illuminated surface areas of photocatalyst.

3D printing of photocatalytic foams [144,145], coupled with computational modelling [146],shows potential in this area, as design of the structures to be printed provides opportunity to increase the surface area which will be illuminated, allowing for bespoke foams to be printed to maximised the efficiency of the reactors. At present, while substrates can be printed with hierarchical foam structures [144], attempts to print substrate free foams are currently limited to simplistic structures. [147, 148].

7. Conclusions

This review of the available literature shows the that photocatalytic foams have the potential to address the limitations of slurries and immobilized catalysts which have, so far, hindered more widespread industrial adoption of photocatalysis for the degradation of organic pollutants in water. Furthermore, studies on their use in continuous flow reactors provide a clear path towards practical adoption. The high performance of foams can be attributed to the combination of favourable physical, e.g. high porosity and surface area, and structural parameters, e.g. mechanical resistance. However, some fundamental gaps still exist, particularly in relation to linking materials' properties to foam performance in photocatalytic flow reactors. The authors encourage the community to focus on key challenges, including:

– Shift the focus from the assessment of surface area, which is relevant for slurries, towards methods to reliably evaluate the active surface, i.e. open porosity which can be reached by the external light source. Characterisation methods like computed tomography (CT) and BET can support these efforts.
– Develop methods to combine the design of the irradiation source and of the foam structure to maximize the active surface, including estimating how deep the irradiation source can penetrate.
– Include assessments of catalyst reusability and long-term performance in scientific publications to facilitate scale-up considerations, including cost.

Furthermore, the field suffers from a lack of common best practices and nomenclature, which makes it challenging comparing performance across different materials, geometries, and process conditions. To address this, the authors have suggested the adoption of:

A clear and simple nomenclature to classify foams based on average pore size and manufacturing process.

The routine use of key figures of merit, including photocatalyst quantum yield and electrical energy per order to compare the performance of different foams under different conditions, moving beyond the mere reporting of degradation rates.

Identification of the nature of the active species within a reaction, such as hydroxyl radicals or superoxide radicals via characterisation such as electron paramagnetic resonance (EPR).

Finally, the authors would like to re-iterate the often-repeated advice that whenever practical or possible, researchers should move away from using dyes, and using HPLC rather than UV-Vis, to determine photocatalytic activity and degradation kinetics.

CRediT authorship contribution statement

Zachary Warren: Conceptualisation, Investigation, Methodology, Visualisation, Writing – original draft. **Thais Tasso Guaraldo:** Conceptualisation, Investigation, Writing – review & editing. **Alysson Stefan Martins:** Conceptualisation, Investigation, Writing – review &

editing. **Jannis Wenk:** Conceptualisation, Supervision, Writing – review & editing. **Davide Mattia:** Conceptualisation, Funding acquisition, Project administration, Supervision, Writing – review & editing.

Declaration of Competing Interest

The authors declare that they have no known competing financial interests or personal relationships that could have appeared to influence the work reported in this paper.

Data Availability

All data used in Appendix.

Appendix A. Supporting information

Supplementary data associated with this article can be found in the online version at doi:10.1016/j.jece.2022.109238.

References

[1] M.N. Chong, et al., Recent developments in photocatalytic water treatment technology: a review, Water Res. 44 (10) (2010) 2997–3027.

[2] S.K. Loeb, et al., The technology horizon for photocatalytic water treatment: sunrise or sunset? Environ. Sci. Technol. 53 (6) (2019) 2937–2947.

[3] C.B.D. Marien, et al., Kinetics and mechanism of Paraquat's degradation: UV-C photolysis vs UV-C photocatalysis with TiO2/SiC foams, J. Hazard. Mater. 370 (December 2017) (2019) 164–171.

[4] Hd Lasa, Photocatalytic Reaction Engineering, Springer US: Imprint, Boston, MA, 2005.

[5] N.A. Kouamé, et al., Preliminary study of the use of β-SiC foam as a photocatalytic support for water treatment, Catal. Today 161 (1) (2011) 3–7.

[6] A. Manassero, M.L. Satuf, O.M. Alfano, Photocatalytic reactors with suspended and immobilized TiO2: Comparative efficiency evaluation, Chem. Eng. J. 326 (2017) 29–36.

[7] S. Horikoshi, N. Serpone, Can the photocatalyst TiO2 be incorporated into a wastewater treatment method? Background and prospects, Catal. Today 340 (August 2018) (2020) 334–346.

[8] V.L. Colvin, The potential environmental impact of engineered nanomaterials, Nat. Biotechnol. 22 (6) (2004), 760-760.

[9] Defra, U.K., Characterising the Potential Risks posed by Engineered Nanoparticles, 2007.

[10] M.A. Kiser, et al., Titanium nanomaterial removal and release from wastewater treatment plants, Environ. Sci. Technol. 43 (17) (2009) 6757–6763.

[11] M.F.J. Dijkstra, et al., Experimental comparison of three reactor designs for photocatalytic water purification, Chem. Eng. Sci. 56 (2) (2001) 547–555.

[12] M.F.J. Dijkstra, et al., Comparison of the efficiency of immobilized and suspended systems in photocatalytic degradation, Catal. Today 66 (2–4) (2001) 487–494.

[13] M. Vargová, et al., TiO2 thick films supported on reticulated macroporous Al2O3 foams and their photoactivity in phenol mineralization, Appl. Surf. Sci. 257 (10) (2011) 4678–4684.

[14] I.J. Ochuma, et al., Three-phase photocatalysis using suspended titania and titania supported on a reticulated foam monolith for water purification, Catal. Today 128 (1–2) (2007) 100–107.

[15] K. Zhang, et al., Self-floating amphiphilic black TiO2 foams with 3D macro-mesoporous architectures as efficient solar-driven photocatalysts, Appl. Catal. B: Environ. 206 (2017) 336–343.

[16] C.B.D. Marien, et al., Kinetics and mechanism of Paraquat's degradation: UV-C photolysis vs UV-C photocatalysis with TiO 2 /SiC foams, J. Hazard. Mater. 370 (December 2017) (2019) 164–171.

[17] M. Vargová, et al., TiO 2 thick films supported on reticulated macroporous Al 2 O 3 foams and their photoactivity in phenol mineralization, Appl. Surf. Sci. 257 (10) (2011) 4678–4684.

[18] K.S.W. Sing, Reporting physisorption data for gas/solid systems with special reference to the determination of surface area and porosity (Recommendations 1984), Pure Appl. Chem. 57 (4) (1985) 603–619.

[19] R.A. Shaw, T. Ogawa, Inorganic polymers. Part I. A solid inorganic foam, J. Polym. Sci. Part A: Gen. Pap. 3 (9) (1965) 3343–3351.

[20] A.R. Studart, et al., Processing routes to macroporous ceramics: a review, J. Am. Ceram. Soc. 89 (6) (2006) 1771–1789.

[21] A. Yamamoto, H. Imai, Preparation of titania foams having an open cellular structure and their application to photocatalysis, J. Catal. 226 (2) (2004) 462–465.

[22] A. Feinle, M.S. Elsaesser, N. Husing, Sol-gel synthesis of monolithic materials with hierarchical porosity, Chem. Soc. Rev. 45 (12) (2016) 3377–3399.

[23] H. Maekawa, et al., Meso/macroporous inorganic oxide monoliths from polymer foams, Adv. Mater. 15 (78) (2003) 591–596.

[24] S. Andrieux, W. Drenckhan, C. Stubenrauch, Highly ordered biobased scaffolds: from liquid to solid foams, Polymers 126 (2017) 425–431.

[25] D. Zabiegaj, et al., Activated carbon monoliths from particle stabilized foams, Microporous Mesoporous Mater. 239 (2017) 45–53.

[26] D. Zabiegaj, et al., Nanoparticle laden interfacial layers and application to foams and solid foams, Colloids Surf. A: Physicochem. Eng. Asp. 438 (2013) 132–140.

[27] M. Costantini, et al., 3D-printing of functionally graded porous materials using on-demand reconfigurable microfluidics, Angew. Chem. - Int. Ed. 58 (23) (2019) 7620–7625.

[28] C. Vakifahmetoglu, D. Zeydanli, P. Colombo, Porous polymer derived ceramics, Mater. Sci. Eng.: R: Rep. 106 (2016) 1–30.

[29] A.N. Kouamé, et al., β-SiC foams as a promising structured photocatalytic support for water and air detoxification, Catal. Today 209 (2013) 13–20.

[30] S.W. da Silva, et al., TiO2 thick films supported on stainless steel foams and their photoactivity in the nonylphenol ethoxylate mineralization, Chem. Eng. J. 283 (2016) 1264–1272.

[31] Y. Xue, et al., Visible light responsive Fe-ZnS/nickel foam photocatalyst with enhanced photocatalytic activity and stability, RSC Adv. 6 (96) (2016) 93370–93373.

[32] M. Kete, et al., Design and evaluation of a compact photocatalytic reactor for water treatment, Environ. Sci. Pollut. Res. 25 (21) (2018) 20453–20465.

[33] F. Cao, Z. Pan, X. Ji, Enhanced photocatalytic activity of a pine-branch-like ternary CuO/CuS/ZnO heterostructure under visible light irradiation, New J. Chem. 43 (28) (2019) 11342–11347.

[34] A. Kocakuşakoğlu, et al., Photocatalytic activity of reticulated ZnO porous ceramics in degradation of azo dye molecules, J. Eur. Ceram. Soc. 35 (10) (2015) 2845–2853.

[35] M. Konyar, et al., Reticulated ZnO photocatalyst: efficiency enhancement in degradation of acid red 88 Azo dye by catalyst surface cleaning, Chem. Eng. Commun. 204 (6) (2017) 705–710.

[36] N. Karimizadeh, et al., Synthesis of three-dimensional multilayer graphene foam/ ZnO nanorod composites and their photocatalyst application, J. Electron. Mater. 47 (9) (2018) 5452–5457.

[37] X. Men, et al., Three-dimensional free-standing ZnO/graphene composite foam for photocurrent generation and photocatalytic activity, Appl. Catal. B: Environ. 187 (2016) 367–374.

[38] E.M. Rangel, C.C.Nd Melo, F.M. Machado, Ceramic foam decorated with ZnO for photodegradation of Rhodamine B dye, Bol. de la Soc. Esp. de Cerámica y Vidr. 58 (3) (2019) 134–140.

[39] K. Pinato, et al., TiO2-coated alveolar clay foam as a photocatalyst for water detoxification, J. Mater. Sci. 55 (4) (2020) 1451–1463.

[40] K. Elatmani, et al., 3D Photocatalytic media for decontamination of water from pesticides, Mater. Res. Bull. 101 (December 2017) (2018) 6–11.

[41] S. Qiu, et al., Synergetic effect of ultrasound, the heterogeneous fenton reaction and photocatalysis by TiO2 loaded on nickel foam on the degradation of pollutants, Materials 9 (2016) 6.

[42] Y. Xue, et al., Visible light responsive Fe–ZnS/nickel foam photocatalyst with enhanced photocatalytic activity and stability, RSC Adv. 6 (96) (2016) 93370–93373.

[43] M. Du, et al., Fluorine doped TiO2/mesocellular foams with an efficient photocatalytic activity, Catal. Today 327 (2019) 340–346.

[44] D. Ding, et al., A simple method for preparing ZnO foam/carbon quantum dots nanocomposite and their photocatalytic applications, Mater. Sci. Semicond. Process. 47 (2016) 25–31.

[45] C.M. Taylor, et al., Enhancing the photo-corrosion resistance of ZnO nanowire photocatalysts, J. Hazard. Mater. 378 (2019), 120799 (March).

[46] K.S.W. Sing, The use of gas adsorption for the characterization of porous solids, Colloids Surf. 38 (1) (1989) 113–124.

[47] B.C. Tappan, S.A. Steiner 3rd, E.P. Luther, Nanoporous metal foams, Angew. Chem. Int. Ed. Engl. 49 (27) (2010) 4544–4565.

[48] N. Serpone, A. Salinaro, Terminology, relative photonic efficiencies and quantum yields in heterogeneous photocatalysis. Part I: Suggested protocol, Pure Appl. Chem. 71 (2) (1999) 303–320.

[49] J. Yu, X. Yu, Hydrothermal synthesis and photocatalytic activity of zinc oxide hollow spheres, Environ. Sci. Technol. 42 (13) (2008) 4902–4907.

[50] T. Peng, et al., Synthesis of titanium dioxide nanoparticles with mesoporous anatase wall and high photocatalytic activity, J. Phys. Chem. B 109 (11) (2005) 4947–4952.

[51] G. Fourie, J, J.P. Du Plessis, Pressure drop modelling in cellular metallic foams, Chem. Eng. Sci. 57 (14) (2002) 2781–2789.

[52] P. Dechadilok, W.M. Deen, Hindrance factors for diffusion and convection in pores, Ind. Eng. Chem. Res. 45 (21) (2006) 6953–6959.

[53] S.A.M. Karimian, A.G. Straatman, CFD study of the hydraulic and thermal behavior of spherical-void-phase porous materials, Int. J. Heat Fluid Flow. 29 (1) (2008) 292–305.

[54] S. Josset, et al., UV-A photocatalytic treatment of Legionella pneumophila bacteria contaminated airflows through three-dimensional solid foam structured photocatalytic reactors, J. Hazard. Mater. 175 (1–3) (2010) 372–381.

[55] G. Plesch, et al., Reticulated macroporous ceramic foam supported TiO2 for photocatalytic applications, Mater. Lett. 63 (3–4) (2009) 461–463.

[56] G. Plesch, et al., Zr doped anatase supported reticulated ceramic foams for photocatalytic water purification, Mater. Res. Bull. 47 (7) (2012) 1680–1686.

[57] H.S. Fogler, Elements of Chemical Reaction Engineering, 3rd ed., 1999.

[58] Z. Warren, et al., Synthesis of photocatalytic pore size-tuned ZnO molecular foams, J. Mater. Chem. A 10 (21) (2022) 11542–11552.

[59] K. Okada, et al., Porous ceramics mimicking nature-preparation and properties of microstructures with unidirectionally oriented pores, Sci. Technol. Adv. Mater. 12 (6) (2011), 064701.

[60] X. Yan, et al., Is methylene blue an appropriate substrate for a photocatalytic activity test? A study with visible-light responsive titania, Chem. Phys. Lett. 429 (4–6) (2006) 606–610.

[61] J.M. Buriak, P.V. Kamat, K.S. Schanze, Best practices for reporting on heterogeneous photocatalysis, ACS Appl. Mater. Interfaces 6 (15) (2014) 11815–11816.

[62] S.E. Braslavsky, Glossary of terms used in photochemistry, 3rd edition (IUPAC Recommendations 2006), Pure Appl. Chem. 79 (3) (2007) 293–465.

[63] J.R. Bolton, et al., Figures-of-merit for the technical development and application of advanced oxidation technologies for both electric- and solar-driven systems (IUPAC Technical Report), Pure Appl. Chem. 73 (4) (2001) 627–637.

[64] A. Ramirez-Canon, et al., Multiscale design of ZnO nanostructured photocatalysts, Phys. Chem. Chem. Phys. 20 (9) (2018) 6648–6656.

[65] N.M. Julkapli, S. Bagheri, Graphene supported heterogeneous catalysts: an overview, Int. J. Hydrog. Energy 40 (2) (2015) 948–979.

[66] F. Li, et al., Graphene oxide: a promising nanomaterial for energy and environmental applications, Nano Energy 16 (2015) 488–515.

[67] P.V. Kamat, Manipulation of charge transfer across semiconductor interface. A criterion that cannot be ignored in photocatalyst design, J. Phys. Chem. Lett. 3 (5) (2012) 663–672.

[68] R. Qiu, et al., Photocatalytic activity of polymer-modified ZnO under visible light irradiation, J. Hazard. Mater. 156 (1–3) (2008) 80–85.

[69] N.M. Gupta, Factors affecting the efficiency of a water splitting photocatalyst: a perspective, Renew. Sustain. Energy Rev. 71 (December 2016) (2017) 585–601.

[70] F. Cao, T. Wang, X. Ji, Enhanced visible photocatalytic activity of tree-like ZnO/CuO nanostructure on Cu foam, Appl. Surf. Sci. 471 (September 2018) (2019) 417–424.

[71] Q. Tong, et al., Preparation and high degradation activity of supported nano-Bi2WO6–TiO2/nickel foam photocatalyst, Nano 10 (2015) 06.

[72] R. He, et al., Room-temperature synthesis of BiOI/Graphene oxide foam composite for phenol removal under visible light, Appl. Surf. Sci. 504 (2020), 144370.

[73] M.F. Ashby, Metal Foams: A Design Guide, Butterworth-Heinemann, Boston, Oxford, 2000.

[74] P. Nguyen, C. Pham, Innovative porous SiC-based materials: From nanoscopic understandings to tunable carriers serving catalytic needs, Appl. Catal. A: Gen. 391 (1–2) (2011) 443–454.

[75] G. Zhang, et al., Photocatalytic oxidation of norfloxacin by Zn0.9Fe0.1S supported on Ni-foam under visible light irradiation, Chemosphere 230 (2019) 406–415.

[76] M. Rico-Santacruz, et al., Alveolar TiO2-β-SiC photocatalytic composite foams with tunable properties for water treatment, Catal. Today 328 (2019) 235–242.

[77] M. Rico-Santacruz, et al., Coating-free TiO2@β-SiC alveolar foams as a ready-to-use composite photocatalyst with tunable adsorption properties for water treatment, RSC Adv. 10 (7) (2020) 3817–3825.

[78] W. Wang, et al., Preparation of 3D network CNTs-modified nickel foam with enhanced microwave absorptivity and application potential in wastewater treatment, Sci. Total Environ. 702 (2020), 135006.

[79] T. Tasso Guaraldo, J. Wenk, D. Mattia, Photocatalytic ZnO foams for micropollutant degradation, Adv. Sustain. Syst. 5 (2021) 5.

[80] R. He, et al., Room-temperature synthesis of BiOI/Graphene oxide foam composite for phenol removal under visible light, Appl. Surf. Sci. (2020) 504.

[81] Y. Zhang, et al., A free-standing 3D nano-composite photo-electrode—Ag/ZnO nanorods arrays on Ni foam effectively degrade berberine, Chem. Eng. J. 373 (2019) 179–191.

[82] P. She, et al., A self-standing macroporous Au/ZnO/reduced graphene oxide foam for recyclable photocatalysis and photocurrent generation, Electrochim. Acta 246 (2017) 35–42.

[83] Y.F. Zhu, L. Zhou, Q.S. Jiang, One-dimensional ZnO nanowires grown on three-dimensional scaffolds for improved photocatalytic activity, Ceram. Int. 46 (1) (2020) 1158–1163.

[84] S. Wu, et al., Biomimetic porous scaffolds for bone tissue engineering, Mater. Sci. Eng.: R: Rep. 80 (2014) 1–36.

[85] J. Banhart, Manufacture, characterisation and application of cellular metals and metal foams, Prog. Mater. Sci. 46 (6) (2001) 559–632.

[86] P. Zhu, Y. Zhao, Mass transfer performance of porous nickel manufactured by lost carbonate sintering process, Adv. Eng. Mater. 19 (2017) 12.

[87] Y. Yamada, et al., Processing of cellular magnesium materials, Adv. Eng. Mater. 2 (4) (2000) 184–187.

[88] E. Solórzano, M.A. Rodriguez-Perez, J.A. de Saja, Thermal conductivity of cellular metals measured by the transient plane source method, Adv. Eng. Mater. 10 (6) (2008) 596–602.

[89] G. Plantard, F. Correia, V. Goetz, Kinetic and efficiency of TiO2-coated on foam or tissue and TiO2-suspension in a photocatalytic reactor applied to the degradation of the 2,4-dichlorophenol, J. Photochem. Photobiol. A: Chem. 222 (1) (2011) 111–116.

[90] Y. Xue, et al., Monolithic nickel foam supported macro-catalyst: manipulation of charge transfer for enhancement of photo-activity, Chem. Eng. J. (2021) 418.

[91] Z. Zeng, D. Jing, L. Guo, Efficient hydrogen production in a spotlight reactor with plate photocatalyst of TiO2/NiO heterojunction supported on nickel foam, Energy (2021) 228.

[92] C. Luo, et al., Preparation of porous micro–nano-structure NiO/ZnO heterojunction and its photocatalytic property, RSC Adv. 4 (6) (2014) 3090–3095.

[93] E.C. Hammel, O.L.R. Ighodaro, O.I. Okoli, Processing and properties of advanced porous ceramics: an application based review, Ceram. Int. 40 (10) (2014) 15351–15370.

[94] B.L. Krasnyi, et al., Chemical resistance of ceramic materials in acids and alkalis, Glass Ceram. 61 (9/10) (2004) 337–339.

[95] H. Cheng, et al., Effect of phase composition, morphology, and specific surface area on the photocatalytic activity of TiO2 nanomaterials, RSC Adv. 4 (87) (2014) 47031–47038.

[96] T. Yildiz, H.C. Yatmaz, K. Öztürk, Anatase TiO2 powder immobilized on reticulated Al2O3 ceramics as a photocatalyst for degradation of RO16 azo dye, Ceram. Int. 46 (7) (2020) 8651–8657.

[97] J.F. Poco, J.H. Satcher, L.W. Hrubesh, Synthesis of high porosity, monolithic alumina aerogels, J. Non-Cryst. Solids 285 (1–3) (2001) 57–63.

[98] K. Prabhakaran, et al., A novel process for low-density alumina foams, J. Am. Ceram. Soc. 88 (9) (2005) 2600–2603.

[99] G. Zu, et al., Preparation and characterization of monolithic alumina aerogels, J. Non-Cryst. Solids 357 (15) (2011) 2903–2906.

[100] T.F. Baumann, et al., Synthesis of high-surface-area alumina aerogels without the use of alkoxide precursors, Chem. Mater. 17 (2) (2004) 395–401.

[101] J.B. Peri, R.B. Hannan, Surface hydroxyl groups on γ-Alumina1, J. Phys. Chem. 64 (10) (2002) 1526–1530.

[102] D. Maciver, Catalytic aluminas II. Catalytic properties of eta and gamma alumina, J. Catal. 3 (6) (1964) 502–511.

[103] J. Reardon, A.K. Datye, A.G. Sault, Tailoring alumina surface chemistry for efficient use of supported MoS2, J. Catal. 173 (1) (1998) 145–156.

[104] J. Cañas, et al., Determination of alumina bandgap and dielectric functions of diamond MOS by STEM-VEELS, Appl. Surf. Sci. 461 (2018) 93–97.

[105] E.O. Filatova, A.S. Konashuk, Interpretation of the changing the band gap of Al2O3 depending on its crystalline form: connection with different local symmetries, J. Phys. Chem. C 119 (35) (2015) 20755–20761.

[106] K. Sivagami, et al., Chlorpyrifos and Endosulfan degradation studies in an annular slurry photo reactor, Ecotoxicol. Environ. Saf. 134 (Pt 2) (2016) 327–331.

[107] A.K. Sharma, R.K. Tiwari, M.S. Gaur, Nanophotocatalytic UV degradation system for organophosphorus pesticides in water samples and analysis by Kubista model, Arab. J. Chem. 9 (2016) S1755–S1764.

[108] R. Moene, et al., Coating of activated carbon with silicon carbide by chemical vapour deposition, Carbon 34 (5) (1996) 567–579.

[109] R. Moene, et al., Conversion of activated carbon into porous silicon carbide by fluidized bedchemical vapour deposition, in: G. Poncelet, et al. (Eds.), Studies in Surface Science and Catalysis, Elsevier, 1995, pp. 371–380.

[110] D. Hao, et al., Synergistic photocatalytic effect of TiO2 coatings and p-type semiconductive SiC foam supports for degradation of organic contaminant, Appl. Catal. B: Environ. 144 (1) (2014) 196–202.

[111] C.B.D. Marien, et al., Kinetics and mechanism of Paraquat's degradation: UV-C photolysis vs UV-C photocatalysis with TiO2/SiC foams, J. Hazard. Mater. 370 (2019) 164–171.

[112] T. Zou, et al., Full mineralization of toluene by photocatalytic degradation with porous TiO2/SiC nanocomposite film, J. Alloy. Compd. 552 (2013) 504–510.

[113] C. Gomez-Solis, et al., Photodegradation of indigo carmine and methylene blue dyes in aqueous solution by SiC-TiO2 catalysts prepared by sol-gel, J. Hazard. Mater. 217–218 (2012) 194–199.

[114] V. Keller, F. Garin, Photocatalytic behavior of a new composite ternary system: WO3/SiC-TiO2. Effect of the coupling of semiconductors and oxides in photocatalytic oxidation of methylethylketone in the gas phase, Catal. Commun. 4 (8) (2003) 377–383.

[115] Y. Su, et al., MOF-derived porous ZnO nanocages/rGO/carbon sponge-based photocatalytic microreactor for efficient degradation of water pollutants and hydrogen evolution, ACS Sustain. Chem. Eng. 6 (9) (2018) 11989–11998.

[116] T. Wang, et al., A facile controllable preparation of highly porous carbon foam and its application in photocatalysis, Mater. Res. Bull. (2020) 122.

[117] M.M. Messina, et al., Simultaneous detection and photocatalysis performed on a 3D graphene/ZnO hybrid platform, Langmuir 36 (9) (2020) 2231–2239.

[118] T. Long, et al., Fabrication of the annular photocatalytic reactor using large-sized freestanding titania-silica monolithic aerogel as the catalyst for degradation of glyphosate, Mater. Des. 159 (2018) 195–200.

[119] A. Yamamoto, Preparation of titania foams having an open cellular structure and their application to photocatalysis, J. Catal. 226 (2) (2004) 462–465.

[120] K.P. Sundar, S. Kanmani, Progression of photocatalytic reactors and it's comparison: a review, Chem. Eng. Res. Des. 154 (2020) 135–150.

[121] Y. Abdel-Maksoud, E. Imam, A. Ramadan, TiO2 solar photocatalytic reactor systems: selection of reactor design for scale-up and commercialization—analytical review, Catalysts 6 (2016) 9.

[122] D. Wang, et al., Engineering and modeling perspectives on photocatalytic reactors for water treatment, Water Res. 202 (2021), 117421.

[123] T.T. Guaraldo, et al., Highly efficient ZnO photocatalytic foam reactors for micropollutant degradation, Chem. Eng. J. (2022).

[124] P.H. Allé, et al., Efficient photocatalytic mineralization of polymethylmethacrylate and polystyrene nanoplastics by TiO2/β-SiC alveolar foams, Environ. Chem. Lett. 19 (2) (2020) 1803–1808.

[125] K. Elatmani, et al., 3D Photocatalytic media for decontamination of water from pesticides, Mater. Res. Bull. 101 (2018) 6–11.

[126] Y. Li, et al., Simulation-guided synthesis of graphitic carbon nitride beads with 3D interconnected and continuous meso/macropore channels for enhanced light absorption and photocatalytic performance, J. Mater. Chem. A 5 (40) (2017) 21300–21312.

[127] Y. Li, et al., In situfabrication of hierarchically porous g-C3N4 and understanding on its enhanced photocatalytic activity based on energy absorption, Appl. Catal. B: Environ. 236 (2018) 64–75.

[128] K. Elatmani, et al., 3D Photocatalytic media for decontamination of water from pesticides, Mater. Res. Bull. 101 (July 2017) (2018) 6–11.

[129] M. Kete, et al., Design and evaluation of a compact photocatalytic reactor for water treatment, Environ. Sci. Pollut. Res. Int. 25 (21) (2018) 20453–20465.

[130] M.E. Leblebici, et al., Computational modelling of a photocatalytic UV-LED reactor with internal mass and photon transfer consideration, Chem. Eng. J. 264 (2015) 962–970.

[131] D. Bertagna Silva, G. Buttiglieri, S. Babic, State-of-the-art and current challenges for TiO2/UV-LED photocatalytic degradation of emerging organic micropollutants, Environ. Sci. Pollut. Res. Int. 28 (1) (2021) 103–120.

[132] D. Bertagna Silva, et al., Impact of UV-LED photoreactor design on the degradation of contaminants of emerging concern, Process Saf. Environ. Prot. 153 (2021) 94–106.

[133] M.M. Khan, et al., Band gap engineered TiO2nanoparticles for visible light induced photoelectrochemical and photocatalytic studies, J. Mater. Chem. A 2 (3) (2014) 637–644.

[134] F. Achouri, et al., Porous Mn-doped ZnO nanoparticles for enhanced solar and visible light photocatalysis, Mater. Des. 101 (2016) 309–316.

[135] I.N. Reddy, et al., Excellent visible-light driven photocatalyst of (Al, Ni) co-doped ZnO structures for organic dye degradation, Catal. Today 340 (May 2018) (2020) 277–285.

[136] B.M. Rajbongshi, A. Ramchiary, S.K. Samdarshi, Influence of N-doping on photocatalytic activity of ZnO nanoparticles under visible light irradiation, Mater. Lett. 134 (2014) 111–114.

[137] M.B. Fisher, et al., Nitrogen and copper doped solar light active TiO2 photocatalysts for water decontamination, Appl. Catal. B: Environ. 130–131 (2013) 8–13.

[138] D.A. Keane, et al., Solar photocatalysis for water disinfection: materials and reactor design, Catal. Sci. Technol. 4 (5) (2014) 1211–1226.

[139] A. Ghosh, A. Mondal, Fabrication of stable, efficient and recyclable p-CuO/n-ZnO thin film heterojunction for visible light driven photocatalytic degradation of organic dyes, Mater. Lett. 164 (2016) 221–224.

[140] Y. Li, et al., Visible-light-driven photocatalytic inactivation of MS2 by metal-free g-C3N4: virucidal performance and mechanism, Water Res 106 (2016) 249–258.

[141] M. Ismael, Y. Wu, A mini-review on the synthesis and structural modification of g-C3N4-based materials, and their applications in solar energy conversion and environmental remediation, Sustain. Energy Fuels 3 (11) (2019) 2907–2925.

[142] J. Xu, Z. Wang, Y. Zhu, Enhanced visible-light-driven photocatalytic disinfection performance and organic pollutant degradation activity of porous g-C3N4 nanosheets, ACS Appl. Mater. Interfaces 9 (33) (2017) 27727–27735.

[143] Q. Zheng, et al., Visible-light-responsive graphitic carbon nitride: rational design and photocatalytic applications for water treatment, Environ. Sci. Technol. 50 (23) (2016) 12938–12948.

[144] Y. de Rancourt de Mimerand, K. Li, J. Guo, Photoactive hybrid materials with fractal designs produced via 3D printing and plasma grafting technologies, ACS Appl. Mater. Interfaces 11 (27) (2019) 24771–24781.

[145] D. Friedmann, et al., Printing approaches to inorganic semiconductor photocatalyst fabrication, J. Mater. Chem. A 7 (18) (2019) 10858–10878.

[146] E. Lee, et al., Design tool and guidelines for outdoor photobioreactors, Chem. Eng. Sci. 106 (2014) 18–29.

[147] S. Son, et al., Customizable 3D-printed architecture with ZnO-based hierarchical structures for enhanced photocatalytic performance, Nanoscale 10 (46) (2018) 21696–21702.

[148] M.J. Martín de Vidales, et al., 3D printed floating photocatalysts for wastewater treatment, Catal. Today 328 (2019) 157–163.